DISCLAIMER NOTICE

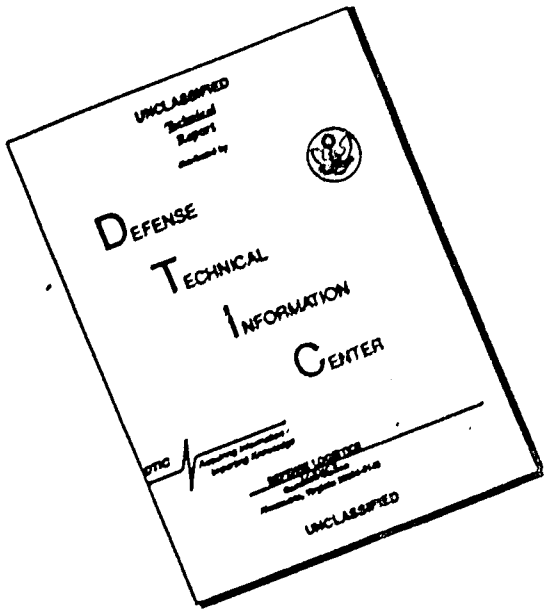

THIS DOCUMENT IS BEST QUALITY AVAILABLE. THE COPY FURNISHED TO DTIC CONTAINED A SIGNIFICANT NUMBER OF PAGES WHICH DO NOT REPRODUCE LEGIBLY.

THE PENNSYLVANIA STATE UNIVERSITY
INSTITUTE FOR SCIENCE & ENGINEERING
UNIVERSITY PARK, PENNSYLVANIA

439631

A Method for the Design of Pumpjets

May 15, 1964

SERIAL NO. NOw 63-0209-c-7

Copy No. 23

NAVY DEPARTMENT • BUREAU OF NAVAL WEAPONS • CONTRACT NOw 63-0209-c

FOR ERRATA

AD 439631

THE FOLLOWING PAGES ARE CHANGES

TO BASIC DOCUMENT

THE PENNSYLVANIA STATE UNIVERSITY
INSTITUTE FOR SCIENCE AND ENGINEERING
ORDNANCE RESEARCH LABORATORY

ADDRESS REPLY TO:
ORDNANCE RESEARCH LABORATORY
P.O. Box 30
STATE COLLEGE, PENNSYLVANIA 16801

JUL 31 1964

To: Attached Distribution List

Subject: Insert for ORL Ext Rept NOw 63-0209-c-7

Reference: (a) ORL Uncl External Report NOw 63-0209-c-7, "A Method for the Design of Pumpjets," 15 May 1964

Enclosure: (1) Paragraph C (Revised), Page 4 of Reference (a)

Gentlemen:

Reference (a) was forwarded to you on 18 May 1964.

Please insert Enclosure (1) on Page 4 of the reference report.

Very truly yours,

ROBERT F. MARBOE
Assistant Director

RFM:njt

C. Improvement of Cavitation Resistance of a Pumpjet

The velocity of flow through a propeller is essentially dictated by the forward velocity of the propelled craft. This velocity of flow is necessarily greater than the velocity which would exist without the propeller present because the flow relative to the propeller is accelerated before it reaches the propeller. A shroud (Fig. 1) reduces the velocity of flow through the pumpjet rotor, thereby making its cavitation characteristics independent, to some extent, of the velocity of the propelled vehicle.

Cavitation in the hydrodynamic propulsor is a function of the velocity of flow relative to the rotating blades of the propulsor. Figure 2 shows a typical inlet velocity diagram for a standard marine propeller and for a pumpjet. Note that the peripheral velocity (U_2) of the propeller blade tip is usually considerably higher than the flow velocity (V_2) through the blades. To reduce the velocity relative to the propeller blades (w_2), the peripheral velocity (U_2) of the blades could be reduced by lowering the rotational speed of the propeller. It is well known that this procedure will

Distribution List

Chief, Bureau of Naval Weapons (RU-2) Department of the Navy Washington 25, D. C.	1 copy	Chief, Bureau of Ships Department of the Navy Washington 25, D. C.	3 copies
Chief, Bureau of Naval Weapons (RUTO-33) Department of the Navy Washington 25, D. C.	2 copies	Commander U. S. Naval Ordnance Laboratory White Oak Silver Spring 19, Maryland	2 copies
Chief, Bureau of Naval Weapons (RUDC) Department of the Navy Washington 25, D. C.	1 copy	Commander U. S. Naval Ordnance Laboratory White Oak Silver Spring 19, Maryland Attn: Dr. S. J. Raff	1 copy
Chief, Bureau of Naval Weapons (RUSD) Department of the Navy Washington 25, D. C.	1 copy	Commander U. S. Naval Ordnance Test Station 3202 East Foothill Boulevard Pasadena Annex Pasadena 8, California	2 copies
Chief, Bureau of Naval Weapons (DLI-3) Department of the Navy Washington 25, D. C.	2 copies		
Chief, Naval Operations (OP 721) Department of the Navy Washington 25, D. C. For: IEP ABC 28	5 copies	Commanding Officer U. S. Naval Underwater Ordnance Station Newport, Rhode Island	2 copies
Chief, Naval Operations (OP 31) Department of the Navy Washington 25, D. C.	1 copy	Commanding Officer U. S. Naval Ordnance Unit Naval Base Key West, Florida	1 copy
Chief, Naval Operations (OP 312) Department of the Navy Washington 25, D. C.	1 copy	Commanding Officer U. S. Naval Torpedo Station Keyport, Washington	1 copy
Chief, Naval Operations (OP 71) Department of the Navy Washington 25, D. C.	1 copy	Commanding Officer U. S. Naval Torpedo Station Quality Evaluation Technical Library Keyport, Washington	1 copy
Chief, Naval Operations (O3EG) Department of the Navy Washington 25, D. C.	1 copy	Director (Code 2021) U. S. Naval Research Laboratory Washington 25, D. C.	3 copies
Chief, Naval Operations (OPO7TC) Technical Analysis and Advisory Group Rm5E613, Pentagon Washington 25, D. C.	1 copy	Director (Code 2027) U. S. Naval Research Laboratory Washington 25, D. C.	1 copy
Chief, Naval Research (Code 411) Department of the Navy Washington 25, D. C.	1 copy	Director U. S. Navy Underwater Sound Reference Laboratory P. O. Box 8337 Orlando, Florida	1 copy
Chief, Naval Research (Code 466) Department of the Navy Washington 25, D. C.	1 copy	Commanding Officer and Director U. S. Navy Electronics Laboratory San Diego 52, California	1 copy
Commander Defense Documentation Center Attention TIPDR Cameron Station Alexandria, Virginia 22314	10 copies 20, 21, 22, 23, 24, 25, 26, 27, 28 & 29	Commanding Officer and Director David Taylor Model Basin Washington 7, D. C.	1 copy

Commanding Officer
U. S. Navy Mine Defense Laboratory
Panama City, Florida — 1 copy

Commanding Officer and Director
U. S. Navy Underwater Sound Laboratory
Fort Trumbull
New London, Connecticut — 1 copy

Commanding Officer and Director
U. S. Navy Marine Engineering Laboratory
Annapolis, Maryland — 1 copy

Commanding Officer and Director
U. S. Naval Training Devices Center
Port Washington, New York — 1 copy

Commander
U. S. Naval Missile Center
Point Mugu
Port Hueneme, California — 1 copy

Commander
U. S. Naval Air Development Center
Johnsville, Pennsylvania — 1 copy

Officer in Charge
Naval Aircraft Torpedo Unit
Naval Air Station
Quonset Point, Rhode Island — 1 copy

Commander, Submarine Force
U. S. Pacific Fleet
c/o Fleet Post Office
San Francisco, California — 1 copy

Commander, Submarine Force
U. S. Atlantic Fleet
c/o P. M. New York, New York — 1 copy

Deputy Commander Submarine Force
U. S. Atlantic Fleet
U. S. Naval Submarine Base New London
Groton, Connecticut — 1 copy

Commander
Submarine Development Group 11
c/o Fleet Post Office
New York, New York — 1 copy

Commander, Cruiser-Destroyer Force
U. S. Pacific Fleet
c/o Fleet Post Office
San Francisco, California — 1 copy

Commander, Destroyer Force
U. S. Atlantic Fleet
Newport, Rhode Island — 1 copy

Commander, Test and Evaluation Force
U. S. Atlantic Fleet
U. S. Naval Base
Norfolk 11, Virginia — 1 copy

Hudson Laboratories
Dobbs Ferry, New York — 1 copy

Commander
Key West Test and Evaluation Detachment
Key West, Florida — 1 copy

Commanding Officer
Advanced Undersea Weapons School
Naval Base
Key West, Florida — 1 copy

Scientific and Technical Information Facility
P. O. Box 5700
Bethesda, Maryland
Attn: NASA Representative (S-AK/DL) — 1 copy

Director, Applied Physics Laboratory
University of Washington
Seattle, Washington — 2 copies

Director, Marine Physical Laboratory
Scripps Institution of Oceanography
San Diego 52, California — 1 copy

Director, Hydrodynamics Laboratory
California Institute of Technology
Pasadena, California — 1 copy

Clevite Ordnance
540 East 105th Street
Cleveland, Ohio — 1 copy

General Electric Company, Ordnance Department
100 Plastics Avenue
Pittsfield, Massachusetts — 1 copy

Director, Davidson Laboratory
Stevens Institute of Technology
711 Hudson Street
Hoboken, New Jersey — 1 copy

Vitro Corporation of America
14,000 Georgia Avenue
Silver Spring, Maryland — 1 copy

Westinghouse Electric Corporation
Landsdowne Plant
Baltimore, Maryland — 1 copy

Woods Hole Oceanographic Institution
Woods Hole, Massachusetts — 1 copy

Aerojet General Corporation
Azusa, California
Attn: G. M. McRoberts — 1 copy

Eastern Research Group
120 Wall Street
New York 5, New York
Attn: Manager — 1 copy

Hydronautics, Inc.
200 Monroe Street
Rockville, Maryland — 1 copy

Institute for Defense Analyses
1666 Connecticut Avenue, N. W.
Washington 9, D. C. — 1 copy

A Method for the Design of Pumpjets

By R. E. Henderson, J. F. McMahon,
and G. F. Wislicenus

The Pennsylvania State University
Institute for Science & Engineering
ORDNANCE RESEARCH LABORATORY
University Park, Pennsylvania

May 15, 1964

APPROVED FOR DISTRIBUTION

George F. Wislicenus

ASSISTANT DIRECTOR

APPROVED FOR DISTRIBUTION

John C. Johnson

DIRECTOR

SERIAL NO. NOw 63-0209-c-7

Distribution List

Chief, Bureau of Naval Weapons (RU-2) Department of the Navy Washington 25, D. C.	1 copy
Chief, Bureau of Naval Weapons (RUTO-33) Department of the Navy Washington 25, D. C.	2 copies
Chief, Bureau of Naval Weapons (RUDC) Department of the Navy Washington 25, D. C.	1 copy
Chief, Bureau of Naval Weapons (RUSD) Department of the Navy Washington 25, D. C.	1 copy
Chief, Bureau of Naval Weapons (DLI-3) Department of the Navy Washington 25, D. C.	2 copies
Chief, Naval Operations (OP 721) Department of the Navy Washington 25, D. C. For: 1EP ABC 28	5 copies
Chief, Naval Operations (OP 31) Department of the Navy Washington 25, D. C.	1 copy
Chief, Naval Operations (OP 312) Department of the Navy Washington 25, D. C.	1 copy
Chief, Naval Operations (OP 71) Department of the Navy Washington 25, D. C.	1 copy
Chief, Naval Operations (O3EG) Department of the Navy Washington 25, D. C.	1 copy
Chief, Naval Operations (OP07TC) Technical Analysis and Advisory Group Rm5E613, Pentagon Washington 25, D. C.	1 copy
Chief, Naval Research (Code 411) Department of the Navy Washington 25, D. C.	1 copy
Chief, Naval Research (Code 466) Department of the Navy Washington 25, D. C.	1 copy
Commander Defense Documentation Center Attention TIPDR Cameron Station Alexandria, Virginia 22314	10 copies
Chief, Bureau of Ships Department of the Navy Washington 25, D. C.	3 copies
Commander U. S. Naval Ordnance Laboratory White Oak Silver Spring 19, Maryland	2 copies
Commander U. S. Naval Ordnance Laboratory White Oak Silver Spring 19, Maryland Attn: Dr. S. J. Raff	1 copy
Commander U. S. Naval Ordnance Test Station 3202 East Foothill Boulevard Pasadena Annex Pasadena 8, California	2 copies
Commanding Officer U. S. Naval Underwater Ordnance Station Newport, Rhode Island	2 copies
Commanding Officer U. S. Naval Ordnance Unit Naval Base Key West, Florida	1 copy
Commanding Officer U. S. Naval Torpedo Station Keyport, Washington	1 copy
Commanding Officer U. S. Naval Torpedo Station Quality Evaluation Technical Library Keyport, Washington	1 copy
Director (Code 2021) U. S. Naval Research Laboratory Washington 25, D. C.	3 copies
Director (Code 2027) U. S. Naval Research Laboratory Washington 25, D. C.	1 copy
Director U. S. Navy Underwater Sound Reference Laboratory P. O. Box 8337 Orlando, Florida	1 copy
Commanding Officer and Director U. S. Navy Electronics Laboratory San Diego 52, California	1 copy
Commanding Officer and Director David Taylor Model Basin Washington 7, D. C.	1 copy

Commanding Officer
U. S. Navy Mine Defense Laboratory
Panama City, Florida
1 copy

Commanding Officer and Director
U. S. Navy Underwater Sound Laboratory
Fort Trumbull
New London, Connecticut
1 copy

Commanding Officer and Director
U. S. Navy Marine Engineering Laboratory
Annapolis, Maryland
1 copy

Commanding Officer and Director
U. S. Naval Training Devices Center
Port Washington, New York
1 copy

Commander
U. S. Naval Missile Center
Point Mugu
Port Hueneme, California
1 copy

Commander
U. S. Naval Air Development Center
Johnsville, Pennsylvania
1 copy

Officer in Charge
Naval Aircraft Torpedo Unit
Naval Air Station
Quonset Point, Rhode Island
1 copy

Commander, Submarine Force
U. S. Pacific Fleet
c/o Fleet Post Office
San Francisco, California
1 copy

Commander, Submarine Force
U. S. Atlantic Fleet
c/o P. M. New York, New York
1 copy

Deputy Commander Submarine Force
U. S. Atlantic Fleet
U. S. Naval Submarine Base New London
Groton, Connecticut
1 copy

Commander
Submarine Development Group 11
c/o Fleet Post Office
New York, New York
1 copy

Commander, Cruiser-Destroyer Force
U. S. Pacific Fleet
c/o Fleet Post Office
San Francisco, California
1 copy

Commander, Destroyer Force
U. S. Atlantic Fleet
Newport, Rhode Island
1 copy

Commander, Test and Evaluation Force
U. S. Atlantic Fleet
U. S. Naval Base
Norfolk 11, Virginia
1 copy

Hudson Laboratories
Dobbs Ferry, New York
1 copy

Commander
Key West Test and Evaluation Detachment
Key West, Florida
1 copy

Commanding Officer
Advanced Undersea Weapons School
Naval Base
Key West, Florida
1 copy

Scientific and Technical Information Facility
P. O. Box 5700
Bethesda, Maryland
Attn: NASA Representative (S-AK/DL)
1 copy

Director, Applied Physics Laboratory
University of Washington
Seattle, Washington
2 copies

Director, Marine Physical Laboratory
Scripps Institution of Oceanography
San Diego 52, California
1 copy

Director, Hydrodynamics Laboratory
California Institute of Technology
Pasadena, California
1 copy

Clevite Ordnance
540 East 105th Street
Cleveland, Ohio
1 copy

General Electric Company, Ordnance Department
100 Plastics Avenue
Pittsfield, Massachusetts
1 copy

Director, Davidson Laboratory
Stevens Institute of Technology
711 Hudson Street
Hoboken, New Jersey
1 copy

Vitro Corporation of America
14,000 Georgia Avenue
Silver Spring, Maryland
1 copy

Westinghouse Electric Corporation
Landsdowne Plant
Baltimore, Maryland
1 copy

Woods Hole Oceanographic Institution
Woods Hole, Massachusetts
1 copy

Aerojet General Corporation
Azusa, California
Attn: G. M. McRoberts
1 copy

Eastern Research Group
120 Wall Street
New York 5, New York
Attn: Manager
1 copy

Hydronautics, Inc.
200 Monroe Street
Rockville, Maryland
1 copy

Institute for Defense Analyses
1666 Connecticut Avenue, N. W.
Washington 9, D. C.
1 copy

Abstract

THE PUMPJET - a hydrodynamic propulsor - is similar to a conventional propeller rotating within a duct or shroud. The shroud permits the flow velocity through the rotor to be controlled more or less independently of the velocity of the vehicle. For certain applications, the pumpjet can be designed to have better cavitation characteristics than an open propeller; alternatively, the pumpjet can be made smaller than the conventional propeller to reduce the weight of the propelling machinery.

The pumpjet may be designed on the basis of knowledge and experience gained from axial-flow compressors and pumps. The meridional flow within the shroud is assumed to be axially symmetrical. The flow through the vane system is considered, with certain restrictions, to be cylindrical. Although axial-compressor data can be used for the blade design, blade profiles suitable for compressors are not suitable for hydrodynamic propulsors because of the stringent requirements regarding cavitation. A quasi one-dimensional method of blade design is described that uses compressor data but still meets the cavitation requirements.

Problems of shroud design, skewed vanes, unsteady force action, and boundary-layer intake are discussed; and problems that remain unsolved are also pointed out.

Table of Contents

List of Illustrations

Nomenclature

A_f = frontal area of propelled vehicle (sq ft)

a = area (sq ft)

C_D = drag coefficient of propelled vehicle = $\dfrac{\text{drag}}{\frac{1}{2}\rho V_0^2 A_f}$

C_L = shroud lift coefficient

C_{L_∞} = blade lift coefficient based on average relative velocity

C_{L_z} = blade lift coefficient based on unit relative velocity

C_m = mass flow coefficient = $\dfrac{\text{mass flow rate}}{\frac{1}{2}\rho V_0 A_f}$

C_Q = torque coefficient = $\dfrac{\text{torque}}{\frac{1}{2}\rho V_0^2 A_f d_0}$

C_T = thrust coefficient = $\dfrac{\text{thrust}}{\frac{1}{2}\rho V_0^2 A_f}$

D = drag of propelled vehicle (lb)

d_0 = maximum diameter of propelled vehicle (ft)

d_p = rotor tip diameter (ft)

F = thrust (lb)

g = dimensional constant = 32.2 $\dfrac{\text{ft-lb mass}}{\text{lb sec}^2}$

h = submergence depth (ft)

H_R = rotor head = $\dfrac{\text{ft-lb}}{\text{lb mass}}$

H_{R_0} = dimensionless rotor head = $\dfrac{H_R}{V_0^2/2g}$

H_{SV} = total inlet head = $\frac{\text{ft-lb}}{\text{lb mass}}$

J = advance ratio = $\frac{V_0}{n d_0}$

L = length of vortex cylinder (ft) (see Fig. 10)

L = length of propelled vehicle (ft)

ℓ = shroud length (ft)

ℓ = blade chord length (ft)

ℓ_a = axial blade chord (ft)

m = mass flow ratio $\left(\frac{\text{slugs}}{\text{sec}}\right)$

m_0 = dimensionless flow rate = $\frac{m}{\frac{\pi}{4}\rho V_1^2 d_P^2}$

n = rotational speed (rps, unless otherwise stated)

n = coordinate normal to streamline (ft)

Δn = offset between mean streamline and camber line measured perpendicular to blade chord (ft)

Δn_i = Δn for NACA 65-series blade operating at $C_{L_\infty} = 1.0$

n_S = specific speed (see equation 23)

n_{P_S} = propulsor specific speed (see equation 26)

Δ_P = difference between blade pressure face and suction face pressure at the same axial position (psf)

p_0 = free-stream static pressure (psf)

p_{cr} = free-stream static pressure at which cavitation appears $\left(\frac{\text{lb}}{\text{sq ft}}\right)$

p_v = vapor pressure of water $\left(\frac{\text{lb}}{\text{sq ft}}\right)$

P = power $\left(\frac{\text{ft-lb}}{\text{sec}}\right)$

Q = volume flow rate (cfs)

R = radial distance from axis of rotation (ft)

r = streamline radius of curvature (ft)

S = suction specific speed (see equation 24)

s = coordinate along streamline (ft)

t = circumferential blade spacing (ft)

U = rotor tip speed (fps)

V = velocity (fps)

V_a = axial component of velocity (fps)

V_m = meridional component of velocity (fps)

V_u = circumferential component of velocity (fps)

V_0 = reference velocity, i.e., forward velocity of propelled vehicle (fps)

V_Γ = velocity induced by shroud (fps)

w = relative velocity (fps)

w_∞ = vectorial average of relative velocity between inlet and exit of blade (fps)

y = coordinate normal to surface (ft)

α = angle of attack

β = blade stagger angle from axial direction

Γ_θ = total circulation resulting from circumferential component of vorticity $\left(\frac{\text{sq ft}}{\text{sec}}\right)$

γ_θ = circulation per unit length resulting from circumferential component of vorticity (fps)

Γ = shroud circulation $\left(\frac{\text{sq ft}}{\text{sec}}\right)$

δ = (defined in Appendix C)

ζ = vorticity $\left(\frac{1}{\text{sec}}\right)$

ζ_R = radial component of vorticity $\left(\frac{1}{\text{sec}}\right)$

ζ_θ = circumferential component of vorticity $\left(\frac{1}{\text{sec}}\right)$

Λ = sweep angle (deg)

η_H = hydraulic efficiency

η_P = propulsive efficiency

η_{RAM} = ram efficiency

θ = boundary-layer momentum thickness (ft)

θ = circumferential direction

ρ = fluid density $\left(\frac{\text{slugs}}{\text{cu ft}}\right)$

σ = cavitation index

σ = skew angle (deg)

τ = circumferential blade thickness (ft)

Subscripts, which indicate stream position, are (see Fig. 1):

1 = upstream of vehicle where the static pressure is equal to the free-stream static pressure far ahead of the propelled vehicle

2 = rotor inlet

3 = rotor exit

4 = downstream of vehicle where the static pressure is equal to the free-stream static pressure far ahead of the propelled vehicle

A Method for the Design of Pumpjets

A. Introduction

A PUMPJET is a rotating hydrodynamic propulsor operating in a close-fitting casing or shroud. It is the hydraulic counterpart of the ducted-fan engine used for aircraft propulsion. The principal difference between a pumpjet and a propeller is the manner in which the fluid flows through the propulsor. The stream of flow through the pumpjet is made to depart from the "natural" or free-stream surface that bounds the flow through a standard propeller. The general form of the departure from the free-stream surface is shown in Fig. 1.

An original purpose of the pumpjet was to improve the cavitation resistance of a hydrodynamic propulsor beyond that of a propeller in the open stream. By the addition of a shroud, the velocity of flow through the pumpjet rotor can be reduced, and its cavitation characteristics become essentially independent of the velocity of the propelled vehicle. As shown in Fig. 1, the diameter of the pumpjet rotor would have to be larger than the propeller to produce the same thrust at the same flow rate through the propeller. This increase in the diameter of the propulsor and the addition of the shroud increase its drag; therefore, the improved cavitation performance is obtained at the expense of propulsor efficiency. The method for obtaining a compromise solution satisfactory for a pumpjet design will be discussed in this report.

It is of interest to observe that the earliest use of a shroud around a hydrodynamic propeller - the "Kort-nozzle" - produced an increase, rather than a decrease, in the velocity of flow through the propeller. The purpose of the Kort-nozzle, however, was only to increase the thrust of a given propeller. As Fig. 1 shows, if the cavitation resistance of the blades is to be improved with no reduction in thrust and with the same rate of flow through the propulsor, the pumpjet rotor must be larger than the propeller.

The pumpjet can also be used to obtain a reduction in the weight of the propulsor by increasing its rotational speed; however, this weight reduction is obtained only at the sacrifice of the cavitation characteristics of the propulsor. With a boundary-layer intake, the process is particularly promising. This application is analagous to aircraft-engine development (1).*

It also appears that the unsteady forces usually associated with propellers operating in the wake of a vehicle may be reduced by the use of the pumpjet; however, there is insufficient understanding of the forces and flow conditions of both propellers and pumpjets to predict the possibilities at this time.

HISTORY OF PUMPJET DESIGN

The idea for using a pumpjet for the suppression of cavitation dates back at least to 1945, at which time G. F. Wislicenus had completed preliminary sketches of an axial-flow pumpjet for the propulsion of torpedoes. The possibility of propelling underwater vehicles with pumpjets was also being considered by others in this field and, as a result, a rather extensive development program was begun at the U. S. Naval Ordnance Test Station (NOTS) in Pasadena. The program explored the use of a radial- or mixed-flow type of pumpjet located at the front of the propelled body to avoid the problem of inlet diffusion.

---

*Numbers in parentheses indicate References listed at end of text.

The possibilities of pumpjet propulsion continued to gain recognition, and a number of significant reports were issued by Dr. Brumfield and his associates at NOTS and by others at the Johns Hopkins University (2, 3). (In reference 2, particular attention is focused on the application of pumpjets to surface ships.) The program at NOTS resulted in some experimental axial-flow pumpjets in the early 1950's. In the mid-1950's, a pumpjet program was begun by the Ordnance Research Laboratory (ORL) at The Pennsylvania State University; this report is concerned primarily with the practical methods of pumpjet design that have been developed at ORL.

Axial-flow compressors for aircraft engines provide a comprehensive background for the design of axial-flow pumpjets (4); however, axial-flow compressors and pumpjets differ in two significant respects.

1. Because the pumpjet operates in a liquid, velocity limits are dictated by cavitation. Although an analogy exists between the flow problems encountered when approaching sonic velocity in a gas and the limits of incipient cavitation in a liquid, the optimum solutions for advancing these limits are not the same for each case.

2. The mechanical problems of blade design for the liquid-handling pumpjet are entirely different from those for the air-handling engine. Bending stresses dominate in the pumpjet; therefore, blades must have relatively low aspect ratios. Centrifugal forces dominate in the air-handling engine (during steady operation); therefore, long, slender blades may be used.

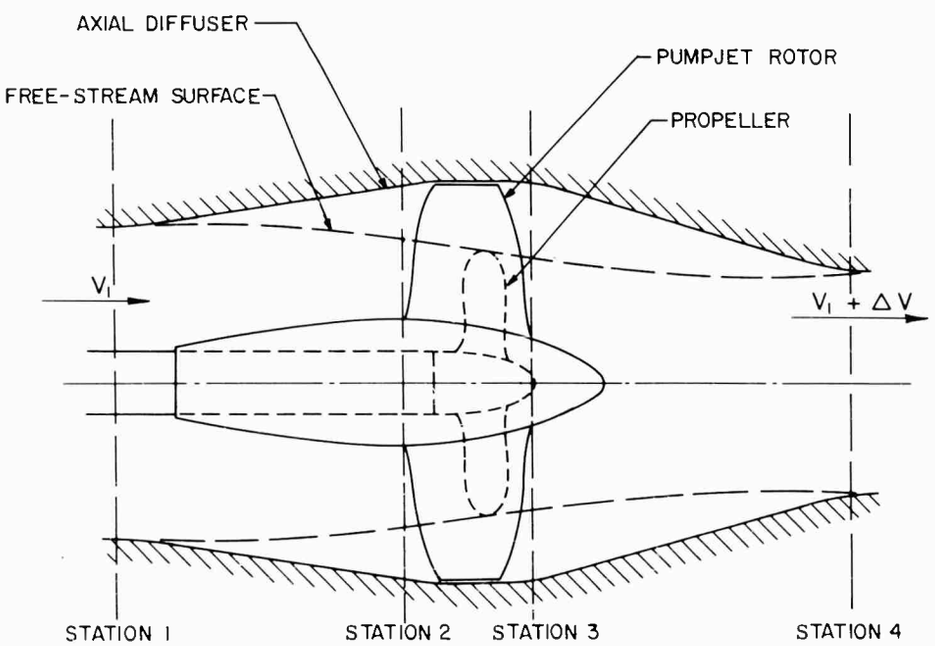

Fig. 1 - Flow Comparison through a Pumpjet and a Propeller

Additional background is also provided by the extensive cavitation experience available from the field of marine propellers and hydrodynamic pumps. The general philosophy of design that is described in this report is based (a) on extensive use of the theoretical and experimental work of NACA and others in the field of axial-flow compressors; (b) on an equally important modification of these aerodynamic developments based on the experience available in the marine-propeller field; and (c) on information available from axial-flow pumps designed for high resistance to cavitation.

B. General Relations for Flow and Force Action

THRUST

The general relations for the flow and force actions of a pumpjet are exactly the same as for those of a propeller. The thrust produced by a propulsor is given by

$$F = \rho Q (V_4 - V_1), \tag{1}$$

where ρ is the fluid density, Q is the volume rate of flow, and V_1 and V_4 are the average velocities in the approach and discharge sections (stations 1 and 4 in Fig. 1). In equation 1 it is assumed that the pressure at station 1 and that at station 4 are both equal to the free-stream pressure at points remote from the propulsor. Under conditions of self-propulsion, the thrust produced by the propulsor is equal to the drag of the propelled craft; therefore, F in equation 1 also represents the total drag of the vehicle at the condition of self-propulsion. In coefficient or nondimensional form, equation 1 may be written:

$$C_T = C_m\left(\frac{V_4}{V_0} - \frac{V_1}{V_0}\right)$$

$$C_D = C_m\left(\frac{V_4}{V_0} - \frac{V_1}{V_0}\right), \tag{2}$$

where C_T is the thrust coefficient, C_D is the drag coefficient (which includes the so-called "thrust deduction"), C_m is the mass-flow-rate coefficient, and V_0 is the forward speed of the vehicle. (A complete definition of these terms is given in the nomenclature.) The equation for C_D in equation 2 is valid only under conditions of self-propulsion.

PROPULSIVE EFFICIENCY

The propulsive efficiency, or propulsive coefficient, is defined as the ratio of the work done by the thrust of the propulsor moving at the velocity V_0 to the energy required to increase the velocity relative to the propulsion unit from V_1 to V_4. If the condition of self-propulsion is considered (i.e., the thrust to the drag equated), then

$$\eta_P = \frac{D V_0}{\frac{1}{2}\rho Q (V_4^2 - V_1^2)}, \tag{3}$$

where D is the drag of the propelled vehicle. If equation 1 is used for the drag, η_P may be written

$$\eta_P = \frac{1}{\frac{V_1}{V_0} + \frac{1}{2}\frac{\Delta V}{V_0}}, \tag{4}$$

where ΔV is equal to $(V_4 - V_1)$. In coefficient form this equation becomes

$$\eta_P = \frac{1}{\frac{1}{2}\frac{C_D}{C_m} + \frac{V_1}{V_0}}. \tag{5}$$

From equation 5 it can be concluded that, for a given vehicle, the higher the mass flow rate the higher the propulsive efficiency. However, it will be seen later in the report that the pumpjet adds an additional drag to the propelled craft, and that this additional drag (or "induced drag"

as it is called) also increases as the mass flow rate increases. Consequently, an optimum mass flow rate exists for any given application.

HEAD, TORQUE, AND POWER RELATIONS

According to Euler's turbomachinery equation, the input energy per pound mass through the propulsor (or head) is given by

$$H_R = \Delta\left[\frac{V_u U}{g}\right], \tag{6}$$

where V_u is the circumferential component of the absolute velocity and U is the circumferential blade velocity. The symbol Δ indicates the difference between the quantity $V_u U$ ahead of the rotor and that behind the rotor. In coefficient form, equation 6 becomes

$$H_{R_0} = 2\Delta\left[\frac{V_u}{V_0}\frac{U}{V_0}\right] \tag{7}$$

It is often found convenient to write this expression

$$H_{R_0} = 2\Delta\left[\frac{V_u}{U}\frac{U^2}{V_0^2}\right] \tag{8}$$

The head may also be written

$$H_R = \frac{1}{2\eta_H}\frac{V_4^2 - V_1^2}{g}, \tag{9}$$

where η_H is the hydraulic efficiency and, consequently, the required power is

$$P = g\rho\, QH_R = \frac{1}{2\eta_H}\rho Q(V_4^2 - V_1^2) \tag{10}$$

In coefficient form, this equation becomes

$$\frac{2\pi}{J} C_Q = \frac{C_D}{\eta_H}\left[\frac{1}{2}\frac{C_D}{C_m} + \frac{V_1}{V_0}\right], \tag{11}$$

where C_Q is the torque coefficient and J is the advance ratio.

By equating relations 6 and 9 (using equation 1) and nondimensionalizing, the following expression is obtained:

$$\Delta\left[\frac{V_u}{U}\frac{U^2}{V_0^2}\right] = \frac{1}{\eta_H}\frac{C_D}{C_m}\left[\frac{1}{2}\frac{C_D}{C_m} + \frac{V_1}{V_0}\right] \tag{12}$$

C. Improvement of Cavitation Resistance of a Pumpjet

The velocity of flow through a propeller is essentially dictated by the forward velocity of the propelled craft. This velocity of flow is necessarily greater than the forward velocity of the vehicle because the flow relative to the propeller is accelerated before it reaches the propeller. A shroud (Fig. 1) reduces the velocity of flow through the pumpjet rotor, thereby making its cavitation characteristics independent, to some extent, of the velocity of the propelled vehicle.

Cavitation in the hydrodynamic propulsor is a function of the velocity of flow relative to the rotating blades of the propulsor. Figure 2 shows a typical inlet velocity diagram for a standard marine propeller and for a pumpjet. Note that the peripheral velocity (U_2) of the propeller blade tip is usually considerably higher than the flow velocity (V_2) through the blades. To reduce the velocity relative to the propeller blades (w_2), the peripheral velocity (U_2) of the blades could be reduced by lowering the rotational speed of the propeller. It is well known that this procedure will

improve the cavitation resistance of the propeller or of a "corresponding pumpjet." (A corresponding pumpjet is defined as one having the same torque, speed, and thrust characteristics as those of a given propeller.)

After the peripheral velocity of the blades has been reduced to a value comparable to the velocity of flow through the blades, further significant reductions in the relative velocity can be realized only by reducing both the axial through-flow velocity and the peripheral velocity of the blades. By adding a shroud, the axial velocity component (V_2) can be reduced to a lower value (V_2') as shown in Fig. 2b. If the peripheral velocity of the blades is reduced correspondingly from U_2 to U_2', the velocity relative to the rotor blades is reduced from w_2 to the lower value w_2'.

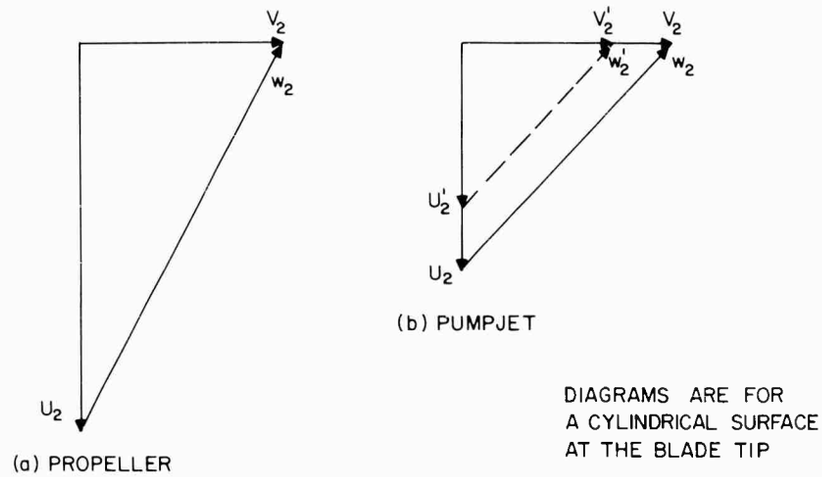

Fig. 2 - Comparison of Typical Inlet Velocity Diagrams for a Standard Marine Propeller and a Corresponding Pumpjet

Because the local pressure reductions at the rotor blades are proportional to w_2^2, the above procedure can substantially improve the cavitation resistance of the rotor. It is essential to note that this improvement can be realized only after the peripheral velocity of the propulsor blades has been reduced to approximately the velocity of flow through the rotor. It has been shown that the relative velocities can be reduced to an extent such that the hull of a vehicle will cavitate before its propulsor blades cavitate (2).

Can retardation of the flow through the propulsor be accomplished without an undue increase in boundary-layer thickness or without actual flow separation? In the aircraft field it has been found that retardations ahead of an unobstructed inlet to a jet engine (Fig. 3) can be quite high, and the resulting so-called "ram" efficiencies are fairly high for flight at low Mach numbers. Since underwater vehicles operate at extremely low Mach numbers, it can be assumed that substantial retardations ahead of a pumpjet inlet can be obtained with good ram efficiencies.

Reference 3 reports on an investigation of inlet retardation or "prediffusion" in cases where the incoming stream includes the boundary layer of the propelled craft. Somewhat unexpectedly it was found that a limited amount of prediffusion is possible even in this case, and that it can be obtained with acceptable ram efficiencies.

D. Over-All Design of an Isolated Pumpjet

The principles of pumpjet design will be discussed first with reference to an isolated pumpjet similar to the jet-engine pod of aircraft (see Fig. 4). For theoretical analysis, the jet engine is

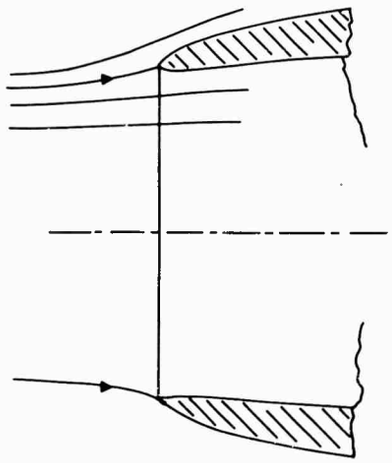

Fig. 3 - Flow Retardation at Shroud Inlet

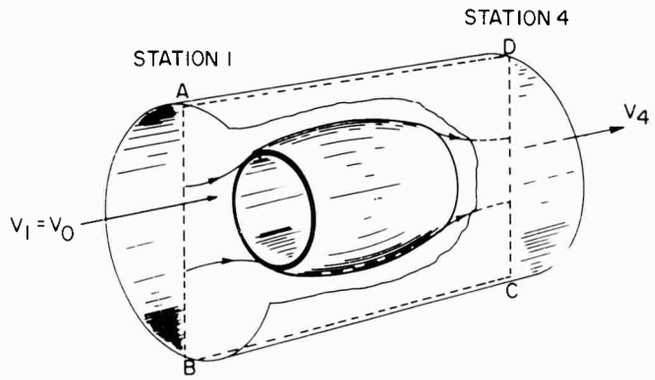

Fig. 4 - Isolated Pumpjet

surrounded by a control volume that is a right cylinder coaxial with the engine. The distance from the surface of this control volume to the engine pod is great enough so that the pressure along the surface of the control volume is equal to the pressure at an infinite distance from the propelled body. Because of axial symmetry, the two-dimensional control area ABCD can be considered rather than the total surface of the control volume.

Equations 1 through 5 apply to the inlet and discharge velocities at stations 1 and 4; the interior of the propulsor, then, has no significance with respect to these over-all relations.

DETERMINATION OF FLOW RATE

The first step in the design is to decide on the rate of volume flow (Q) of the pumpjet. From equation 5, it is apparent that the larger this rate of volume flow, the better will be the propulsive efficiency of the pumpjet; therefore, as the diameter of the pumpjet is increased, less excess velocity must be left in its wake to produce the required thrust.

Because the external-friction drag of the pumpjet is part of the over-all drag of the propelled vehicle, this drag must be deducted from the thrust (as expressed by equation 1) to determine the thrust exerted by the pumpjet. As the frontal area of the pumpjet is increased, this external-friction drag will increase.

Figure 5 is a "carpet" plot of the propulsive efficiency of a jet engine or pumpjet (as expressed by equation 4); however, the curves are corrected for the friction drag of the shroud or casing. The curves for progressively increasing values of duct-loss coefficient k are separated from each other by a horizontal shift of the $\Delta V/V_1$ scale toward the left in direct proportion to the duct-loss coefficient. The curve k = 0 represents the ideal case of zero friction drag on the shroud, i.e., an unshrouded propeller; therefore, it is identical with the propulsive coefficient expressed by equation 4. The numbers on the curves represent that portion of the kinetic energy of the incoming flow per unit mass of fluid passing through the pumpjet that may be regarded as being lost by the friction drag on the shroud or casing. If only 10 per cent of the kinetic energy of the incoming flow were lost in this manner, the maximum propulsive efficiency would drop to approximately 75 per cent and the ratio of velocity increase through the pumpjet for optimum efficiency would change from $\Delta V/V_1 = 0$ for the unshrouded propeller in the open stream to $\Delta V/V_1 = 0.3$ for a pumpjet. Actually, more than 10 per cent of the kinetic energy of the incoming stream is expected to be lost because of the over-all friction of the shroud. Accordingly, Fig. 5 indicates that the maximum propulsive efficiency, corrected for the added drag of the shroud, is to be expected at velocity-increase ratios $\Delta V/V_1$ in excess of 0.3, presumably leading to optimum values for this ratio between 0.3 and 0.6. Although the true value of k cannot be reliably estimated before the pumpjet is designed, a value of $\Delta V/V_1$ in the range indicated above should result in a favorable efficiency of the over-all unit. It should be recognized that, in general, this ratio will be chosen as high as can be justified on the basis of efficiency considerations given before. As can be seen from equation 1, with higher values of ΔV less mass flow is required to produce a certain thrust; therefore, the diameter of the pumpjet can be kept smaller.

From the standpoint of over-all efficiency, then, a pumpjet should be smaller than a corresponding propeller - in contrast to the opposite relationship for the same mass flow rate. The fact that the pumpjet should be smaller than a corresponding propeller can generally be used to estimate the diameter of a pumpjet to take the place of an existing propeller. A pumpjet with a rotor diameter about 15 or 20 per cent less than that of a corresponding propeller is a suitable starting point for a process of iteration leading to a suitable size for a given application.

PRELIMINARY SHROUD DESIGN

After the mass flow rate of the pumpjet has been determined, the casing or shroud may be designed on the basis of one-dimensional considerations of continuity of the flow between the shroud and the central body of the propulsor. The shape of this central body is usually determined by some mechanical considerations of the rotating mechanism. Stream surfaces of revolution may be drawn around the central body based on a certain mean velocity of flow between the upstream surface and the central body. The rate of volume flow is that given by the preceding considerations and equation 1. The line marked 1 on Fig. 6 represents a stream surface of revolution corresponding to the velocity inflow (V_1) well ahead of the shroud. The line marked 1' represents the stream surface corresponding to a velocity (V_1') somewhat lower than V_1 in accordance with the expected retardation before the fluid enters the propulsor. Correspondingly, the stream surface marked 2 represents the stream surface corresponding to a velocity V_2 at the inlet of the rotor sufficient to allow the required volume flow (Q) to pass between this stream surface and the central body of the unit. The stream surfaces marked 3 and 4' are likewise defined according to continuity considerations at the trailing edge of the rotor and at the shroud discharge, respectively.

A first estimate of the inside contour of the shroud may now be drawn as follows: at the inlet, the surface must be slightly outside the stream surface 1'; it should pass through the stream surfaces 2 and 3 near the estimated inlet and discharge of the rotor (stations 2 and 3); and it must end slightly outside the stream surface 4' because the contraction of the contour toward the discharge end of the shroud will produce a slight "vena contracta" for the discharging jet.

As yet, no consideration has been given to the length of the shroud, i.e., the longitudinal distance between stations 1' and 4'. Some indication of this length may be obtained on the basis of mechanical considerations and the location and general arrangement of the pumpjet relative to the propelled vehicle; however, a hydrodynamic criterion will be discussed at the end of this section. Figure 6 also shows a very simple geometric flow criterion that involves the angle of attack between the

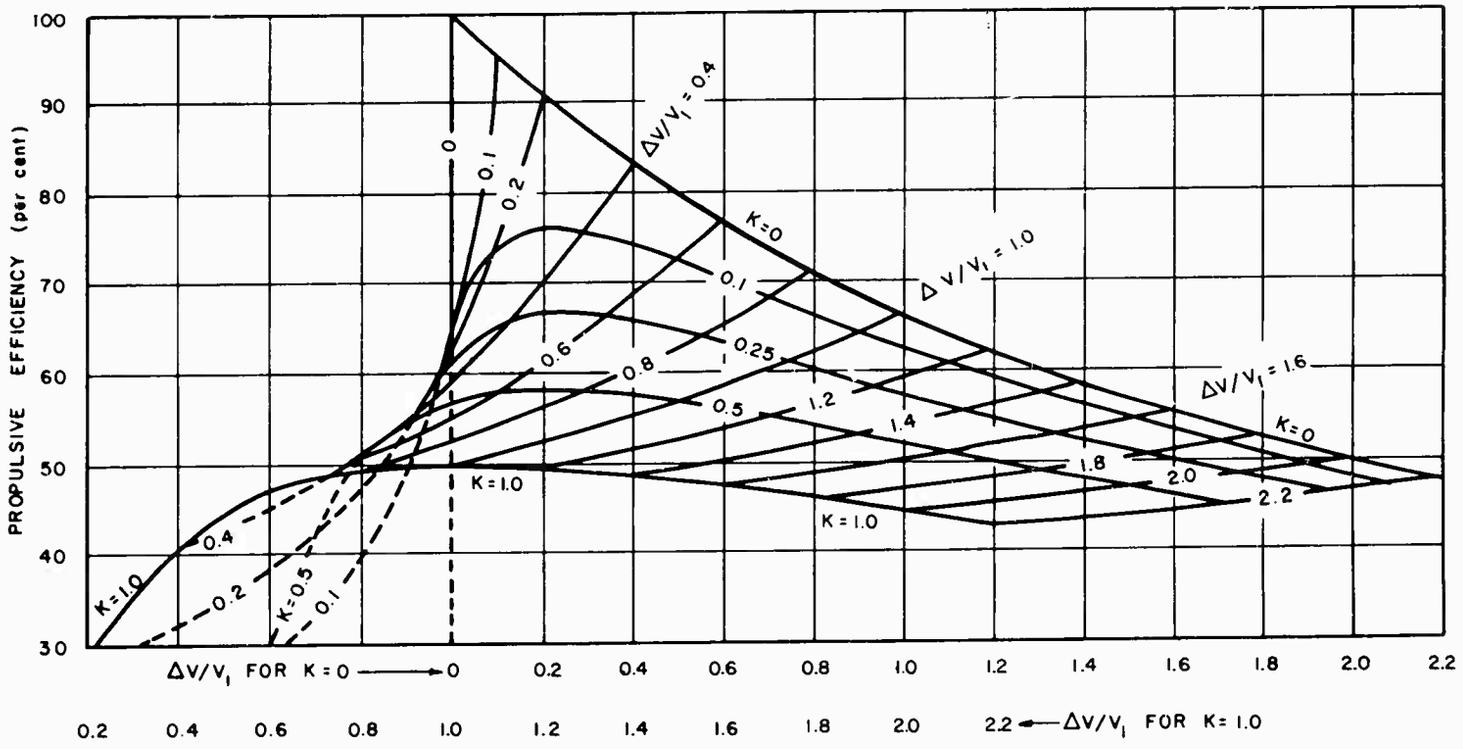

Fig. 5 - Propulsive Efficiency of a Pumpjet for Several Values of Duct-Loss Coefficient

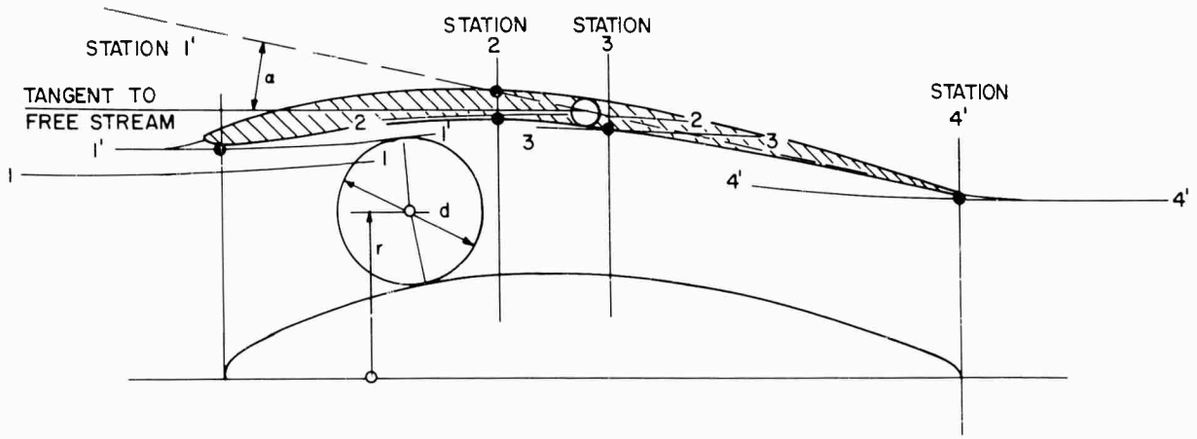

Fig. 6 - Fluid Flow through Shroud with Rotor Not Operating

undisturbed flow (the flow that would exist - without the shroud - at the approximate geometric center of the shroud) and a zero lift line obtained by drawing a straight line between the trailing edge and the center of the shroud profile (with finite thickness). It will be recognized that this approximation of the zero lift direction is taken from plane flow considerations of airfoils and cannot be considered as exact for a ring airfoil (the shroud of the pumpjet). By analogy to plane-airfoil flow, it is possible to use the approximation that the lift coefficient is roughly equal to one-tenth the angle of attack, α, measured (in degrees) from the zero lift direction. Thus, if a lift coefficient of 1.5 is considered to be a limit obtainable without separation, the angle α, as shown in Fig. 4, should not exceed 15 deg. Despite the relative crudeness of this approximation, considerations of this type have led to practical results.

FLOW BETWEEN THE SHROUD AND THE CENTRAL BODY

The meridional flow between the central body and the shroud designed as discussed above is not uniform because it is influenced by the curvature of the flow. Figure 7 shows a simple graphical approximation for the velocity distribution, V_m, between the shroud and the central body. This approximation is obtained on the basis of the radius of curvature of the boundaries at the outer and the inner end of the flow cross section. The equation used is for irrotational fluid motion:

$$\frac{\partial V_m}{\partial n} + \frac{V_m}{r} = 0 \,, \qquad 13$$

where n is the coordinate normal to the flow, and r is the radius of curvature of the streamlines. A start can be made with the radii of curvature, r_o and r_i, at the outer and inner boundaries of the flow and radii of curvature can be obtained for intermediate streamlines by a process of iteration.

REFINEMENT OF SHROUD DESIGN

Before the next step in the design process is described (i.e., the placing of at least one rotating and one stationary vane system into the stream between the shroud and the central body), the previously mentioned problem of the hydrodynamic effects of the shroud should be reconsidered. It was mentioned that the consideration of shroud angle of attack (α) is rather crude and not acceptable as a final solution. References 5 and 6 present theoretical approaches to this problem; however, one of the most practical solutions may be that of McCormick and Eisenhuth (7), which is based, quite logically, on the difference in the diameter of a pumpjet rotor and that of a corresponding propeller.

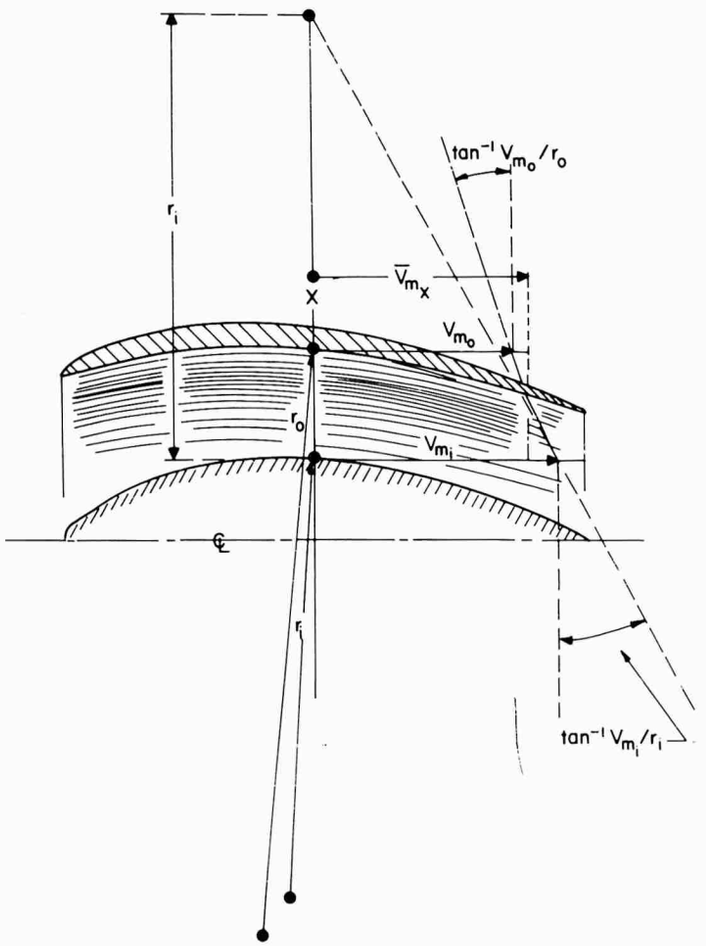

Fig. 7 - Approximation of Velocity Distribution between the Shroud and the Central Body

It may be of interest that the circulation around the shroud of a pumpjet can be approximated by one-dimensional considerations of the flow between the shroud and the central body. Figure 8 shows the configuration considered. The central body is of a more conventional shape than that previously discussed; i.e., it could represent either the central body of an isolated pumpjet (where the through flow may be considered irrotational) or the after end of a propelled vehicle (where the through flow can no longer be considered irrotational because the propulsor is immersed in the boundary layer of the vehicle).

The shroud effect is considered here with no thought of the effect of the pumpjet rotor; therefore, the flow considered here differs from the flow under actual operating conditions in the manner indicated by Fig. 9. This figure indicates that, with no pump rotor in the shroud, the flow leaving and entering the space between the shroud and the central body has the same velocity in the inlet station a_i^*, as it has in the discharge station a_{ex}, as long as the distances from these stations to the shroud are sufficiently great such that the shroud does not influence the pressure at either section. (The effect of the propelled body on the velocity and pressure is ignored.) The inlet streamline S^*, therefore, is different from the streamline S that exists with the pumpjet operating. As a result, with the pumpjet operating, a higher velocity is produced at station a_{ex} than at a_i^*. The circu-

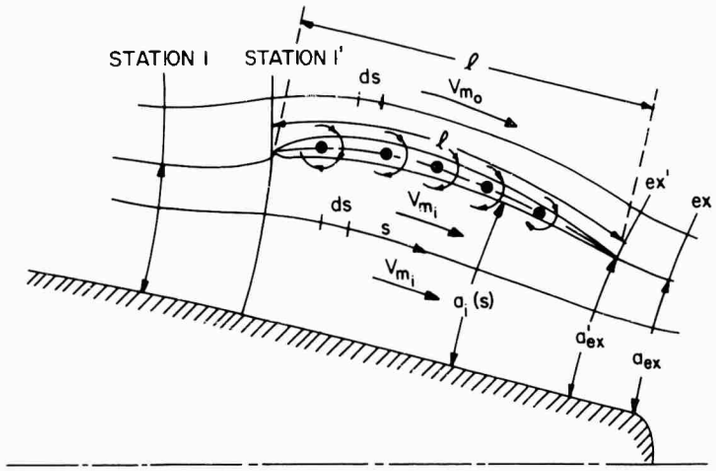

Fig. 8 - Shroud Circulation

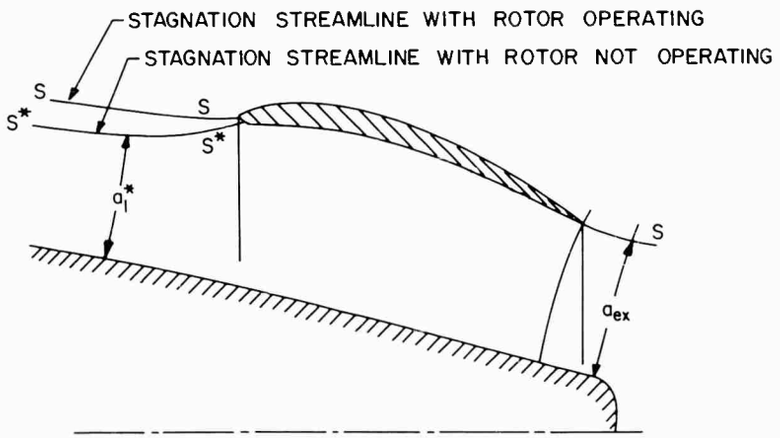

Fig. 9 - Effect of Pumpjet Rotor on Flow at Shroud Inlet

lation approximated on the basis of a shroud without a pumpjet rotor is, therefore, larger than the circulation calculated when the action of the pumpjet rotor is considered.

Under the above conditions, the circulation around the shroud without a rotor (see Fig. 8) is

$$\Gamma = \int_1^{ex} V_{m_o} \, ds - \int_1^{ex} V_{m_i} \, ds \qquad 14$$

A one-dimensional approximation is obtained by putting $V_{m_i} = \overline{V_{m_i}}$, where $\overline{V_{m_i}}$ is the mean velocity of a meridional flow through any flow section between the shroud and the central body. For V_{m_o}, the following approximation can be used:

$$V_{m_o} - V_0 = V_0 - \overline{V_{m_i}} \quad , \qquad 15$$

where $\overline{V_{m_i}}$ is determined with no pumpjet rotor. The term $\overline{V_{m_i}}$ may be estimated as

$$\overline{V_{m_i}} = V_0 \frac{a_{ex}}{a_i(s)} \quad , \qquad 16$$

where $a_i(s)$ is any cross section inside the shroud and is a function of the distance (s) along the flow through this space.

In equation 14, the parts of the integrations that fall between stations 1 and 1' ahead of the shroud and the stations ex' and ex behind the shroud must necessarily vanish because the flow may be regarded as irrotational in these regions.

Thus, the lengths of these integrations may be reduced to the distances between the sections 1' and ex' and are approximated by the length of the shroud, ℓ. With this approximation and the mean values of the velocities along the streamlines shown in Fig. 8, a first approximation of the circulation around the shroud without a pumpjet rotor can be obtained:

$$\Gamma = \ell(\overline{V_{m_o}} - \overline{\overline{V_{m_i}}}) , \tag{17}$$

where one bar above the velocity symbol means an average value in the direction of the flow and two bars indicate averages - both in the direction of the flow and over the cross section of the flow.

From equation 15

$$\overline{V_{m_o}} = 2V_0 - \overline{V_{m_i}} , \tag{18}$$

therefore,

$$\Gamma = 2\ell(V_0 - \overline{\overline{V_{m_i}}}) . \tag{19}$$

By using the usual relationship between the lift coefficient and the circulation, the following approximation can be obtained for the lift coefficient of the shroud without the pumpjet rotor operating:

$$C_L = \frac{2\Gamma}{\ell V_0} = \frac{4\ell(V_0 - \overline{\overline{V_{m_i}}})}{\ell V_0}$$

or

$$C_L = 4\left\{1 - \frac{\overline{\overline{V_{m_i}}}}{V_0}\right\} . \tag{20}$$

Because of the previous definition of $\overline{\overline{V_{m_i}}}$, it is possible to write the following expression for an average flow cross section between the shroud and the central body within the flow regime considered:

$$\overline{\overline{V_{m_i}}}\ \overline{o_i} = o_{ex}\, V_0 , \tag{21}$$

and, using the obvious relationship,

$$\frac{\overline{\overline{V_{m_i}}}}{V_0} = \frac{o_{ex}}{\overline{o_i}} ,$$

the final result obtained is:

$$C_L = 4\left\{1 - \frac{o_{ex}}{\overline{o_i}}\right\} . \tag{22}$$

Because the free-stream discharge cross section (a_{ex}) may be related to the discharge cross section between the shroud and the central body (a_{ex}') by the empirical coefficients for a vena contracta, it is possible to obtain a first approximation for the lift coefficient - in accordance with equation 22 - on the basis of the average cross section between the shroud and the central body compared with the discharge cross section (a_{ex}') of the same stream. Although this solution is approximate, because the action of the pumpjet rotor has been neglected, the results are on the safe side.

The shroud lift coefficient is of interest because it can provide an estimate of the possibility of flow separation on the outside contour of the shroud. If the lift coefficient calculated by this one-dimensional approximation (equation 22) is not greater than approximately 1.5, it may be concluded that there is little likelihood of separation.

The use of a one-dimensional consideration for the flow between the shroud and the central body must be challenged because the circulatory action of the shroud cannot possibly be uniform with respect to the flow between the shroud and the central body. To determine the accuracy of this approximation, the flow induced by a cylindrical distribution of ring vortices was determined. Figure 10 shows the velocity at the two ends and at the middle of the ring vortex cylinder for L = 2R, where L is the length of the vortex cylinder and R is its radius. Figure 11 shows the same velocity distributions for L = R. In the latter case, the maximum change in the induced velocity between the centerline of the system and the vortex cylinder is approximately 37 per cent of the maximum induced velocity in the middle of the vortex cylinder and is far less at its ends. For L = 2R, the nonuniformity in velocity is approximately 14 per cent of the maximum induced velocity in the middle of the vortex cylinder and, again, is far less at its ends. It is evident (Fig. 12) that the percentage of variation of the actual through-flow velocity in the space between the shroud and the central body is considerably less than the ratio of the resultant velocity (V_m) inside the shroud to the induced velocity of the vortex cylinder (V_r) It is concluded that a relatively simple approximation for the nonuniformities of the velocity distribution between the shroud and the central body, such as is indicated by Fig. 7 and equation 20, is probably sufficient for most practical design problems. It will be seen in the following section of this report that the influence of nonuniformities in velocity ahead of the inlet to the pumpjet far overshadows that of the nonuniformities in velocity induced by the shroud.

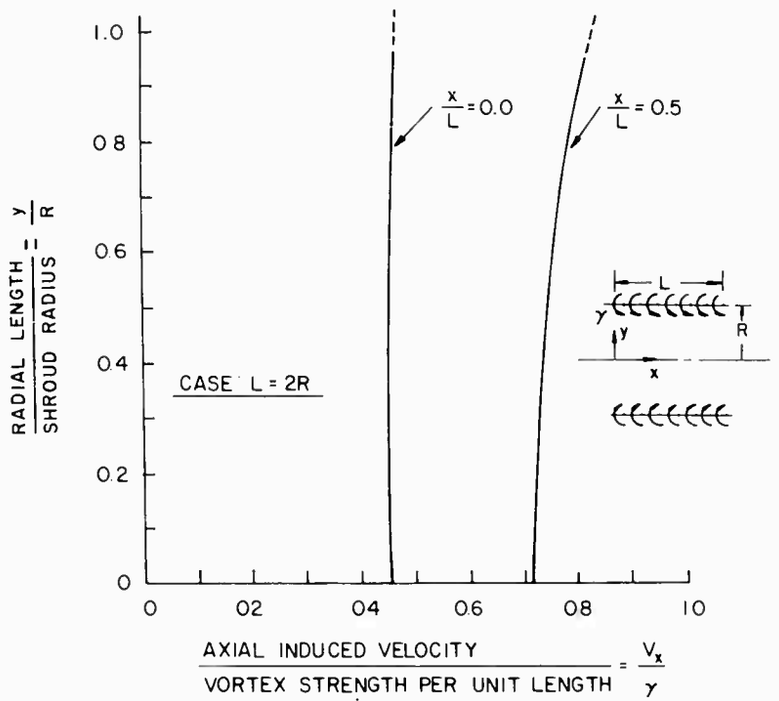

Fig. 10 - Velocity Induced by Ring Vortex Cylinder for L = 2R

It should be recognized that an opinion regarding the danger of separation over the external shroud surface cannot be formed solely from the one-dimensional approximation of the lift coefficient, as expressed by equation 22, because it does not contain the ratio of the length of the shroud to its radius or diameter. However, this lift coefficient, and the angle of attack defined by Fig. 6, may enable the designer to avoid conditions under which separation is to be expected. The actual problem of separation over a ring-shaped lifting surface, such as a shroud of this type, is a rather involved problem of three-dimensional boundary-layer flow (8).

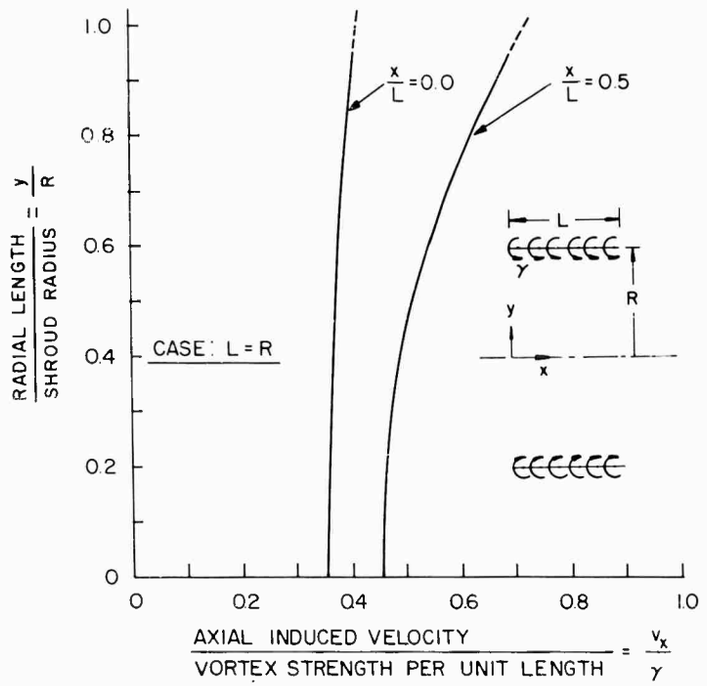

Fig. 11 - Velocity Induced by Ring Vortex Cylinder for L = R

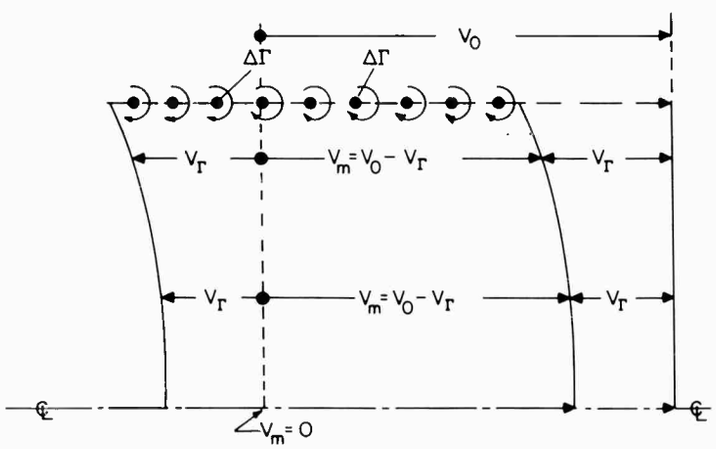

Fig. 12 - Effect of Shroud on Through Flow

E. Over-All Design Considerations for the Speed of Rotation

The following considerations are a part of the over-all design considerations of a pod-type pumpjet and are distinct from the preceding considerations because the prior discussion did not include the pumpjet rotor. The material that has been presented in Section D would remain

essentially the same if the energy addition to the stream between the shroud and the eentral body were aecomplished by a suitable jet pump rather than by a rotating pump impeller. In this report, however, this means of energy addition is not considered.

ADVANCE RATIO

For a pumpjet of given through-flow characteristics, as previously discussed, the speed of rotation ean be determined by assuming a certain "advanee ratio," which is proportional to the ratio of the axial or through-flow velocity to the peripheral velocity of the rotating element. It was stated in Section A that this advance ratio should be as high as possible to achieve optimum cavitation characteristics; however, such a choice results in a fairly low speed of rotation, which requires rather large and heavy propulsion machinery (9). Furthermore, with a low rotational speed there exists the danger of flow separation within the rotor-and-vane system since, according to equation 6, a low blade velocity (U) implies a high value of V_u for a specific energy input. Therefore, low rotational speeds result in large flow deflections within the rotor (especially near the root of the blades) and the resulting possibility of flow separation.

SPECIFIC SPEED

Following standard compressor practice, it is tempting to solve this problem by a process of trial and error; i. e., attempt to design the blade system for an assumed advance ratio and then change the assumption, by successive steps, to achieve a satisfactory design solution. The methods employed in this process are discussed in detail later in the report. This trial-and-error process can be appreciably shortened by using information available from pump designs. The pump designer characterizes all geometrically similar machines by their operating characteristics in terms of the so-called "specific speed" of the machine; therefore, before designing a machine, its general form and characteristics can be estimated by calculating its specific speed:

$$n_S = \frac{n\sqrt{Q}}{H^{3/4}} \quad . \tag{23}$$

In this equation, n is the rotational speed in revolutions per minute; Q is the total volume rate of flow through the unit in gallons per minute; and $H = H_R/\eta_H$, where η_H is the hydraulic efficiency and H_R is the pump head in foot-pounds per pound mass (i.e., the work input for every pound mass of fluid flowing through the machine). For a pumpjet, the head is equal to the increase in kinetic energy between the inlet and discharge streams of the unit as given in equation 9.

The specific speed usually used in pump design (equation 23) could be made dimensionless by multiplying it by a dimensional constant. As a dimensionless characteristic of the machine, it is related to the dimensionless flow characteristics within the machine, such as the advance ratio previously mentioned and the pressure or head coefficient of the rotor-and-vane system (which determines the flow deflection in the system and, to some extent, the possibility of separation). These derivations are fully covered in Section B of this report and in Section 10 of reference 10.

On the bases of the considerations given in reference 10, and the empirical knowledge available in the field, the specific speeds of single-stage axial-flow pumps should be kept between values of 6000 and 11,000 (with the dimensions as given above). Values lower than 6000 result either in excessive deflections of the flow in the root sections of the rotor blades or in an excessively large hub or root diameter. Values of thc specific speed in excess of 11,000 imply velocities that are high compared to the pump head (actually the square of the velocity is compared to the pump head) and, consequently, result in low over-all efficiencies. Since a radially nonuniform head can be used for pumpjets, it may be possible to employ specific speeds lower than 6000, but the design must then depart somewhat from the conventional practice of pump design.

SUCTION SPECIFIC SPEED

By similarity considerations quite analogous to those that have led to the specific speed, an over-all judgment of the cavitation problem involved in a specific application can be obtained before the pumpjet is actually designed. The cavitation characteristics of hydrodynamic machines can be expressed by the so-called "suction specific speed":

$$S = \frac{n\sqrt{Q}}{H_{SV}^{3/4}} , \qquad 24$$

where H_{SV} is the so-called "total inlet head" (the energy in foot-pounds per pound mass of incoming stream that exceeds the vapor pressure of the liquid), and n and Q have the same dimensions as in equation 23. For a propeller or a pumpjet, this inlet head is

$$H_{SV} = h + 31 + \eta_{RAM} \frac{V_1^2}{2g} , \qquad 25$$

where h is the depth, in feet, of the propulsor below the surface of the ocean; the constant 31 is the atmospheric pressure minus the vapor pressure of cold water expressed in feet of sea water; and η_{RAM} is the ram efficiency (i.e., the per cent of the inlet kinetic energy available at the pump rotor). This efficiency can be 80 per cent or higher for a well-designed inlet, even if the velocity distribution at the inlet is not uniform (3).

The suction specific speed can also be related to the flow conditions inside the machine as shown by Fig. 13 (which is derived from Fig. 37 of reference 10). The figure shows curves of constant values of the pressure or cavitation coefficient of the blades with respect to the velocity of flow relative to the moving blades. The curve of suction specific speed that can be obtained for an assumed blade coefficient has a fairly flat optimum when plotted against the advance ratio (V_m/U) of the rotor tip section. Since cavitation-free performance has been achieved with blade cavitation numbers (C_b) as low as 0.2, it can be concluded from Fig. 13 that suction specific speeds up to about 10,000 can be achieved under conditions where cavitation must be completely avoided, although such a value will require a very precise blade design. If some local cavitation is tolerable, substantially higher suction specific speeds can be achieved.

It can also be seen from Fig. 13 that the advance ratio of the rotor tip section must be between 0.25 and 0.35 to obtain a suction specific speed of 10,000 with a blade pressure coefficient of not less than 0.2. If it is desirable to maintain a reasonably high speed of rotation, the advance ratio cannot be chosen simply as low as possible (as might be indicated by only cavitation considerations), but the advance ratio has an optimum dictated by the inlet operating conditions as expressed by the suction specific speed.

On the bases of equations 9 and 25, it is relatively easy to form an opinion about the total inlet head (H_{SV}) in comparison with the head (H_R) of the pumpjet. For example, if V_4 were larger than V_1 by the factor $\sqrt{2}$, equation 9 would show the pump head to be $V_1^2/2g$. From equation 25, it is evident that H_{SV} generally will be larger than $V_1^2/2g$ and, therefore, generally larger than the pump head (H_R). Thus, the suction specific speed for jet pumps is usually lower than the specific speed of the machine; and it can be concluded that it is generally possible to avoid incipient cavitation in pumpjets within the specific-speed range mentioned above (6000 to 11,000).

It should be noted that the relationship between the suction specific speed and the other flow characteristics given in Fig. 13 is based on the assumption of a rotor hub diameter of zero. In reality, the suction specific speeds will be lower by the square root of the actual inflow cross section of the rotor as compared with $D_2^2 \pi/4$, where D_2 is the inlet tip diameter of the rotor. This reduction in suction specific speed is small unless the diameter of the hub is larger than the radius of the rotor tip.

PROPULSOR SPECIFIC SPEED

It should be noted that the foregoing similarity considerations should actually be expressed directly in terms of the operating conditions that are of importance for pumpjet performance. For example, instead of using the volume rate of flow and the head of the machine, it would certainly

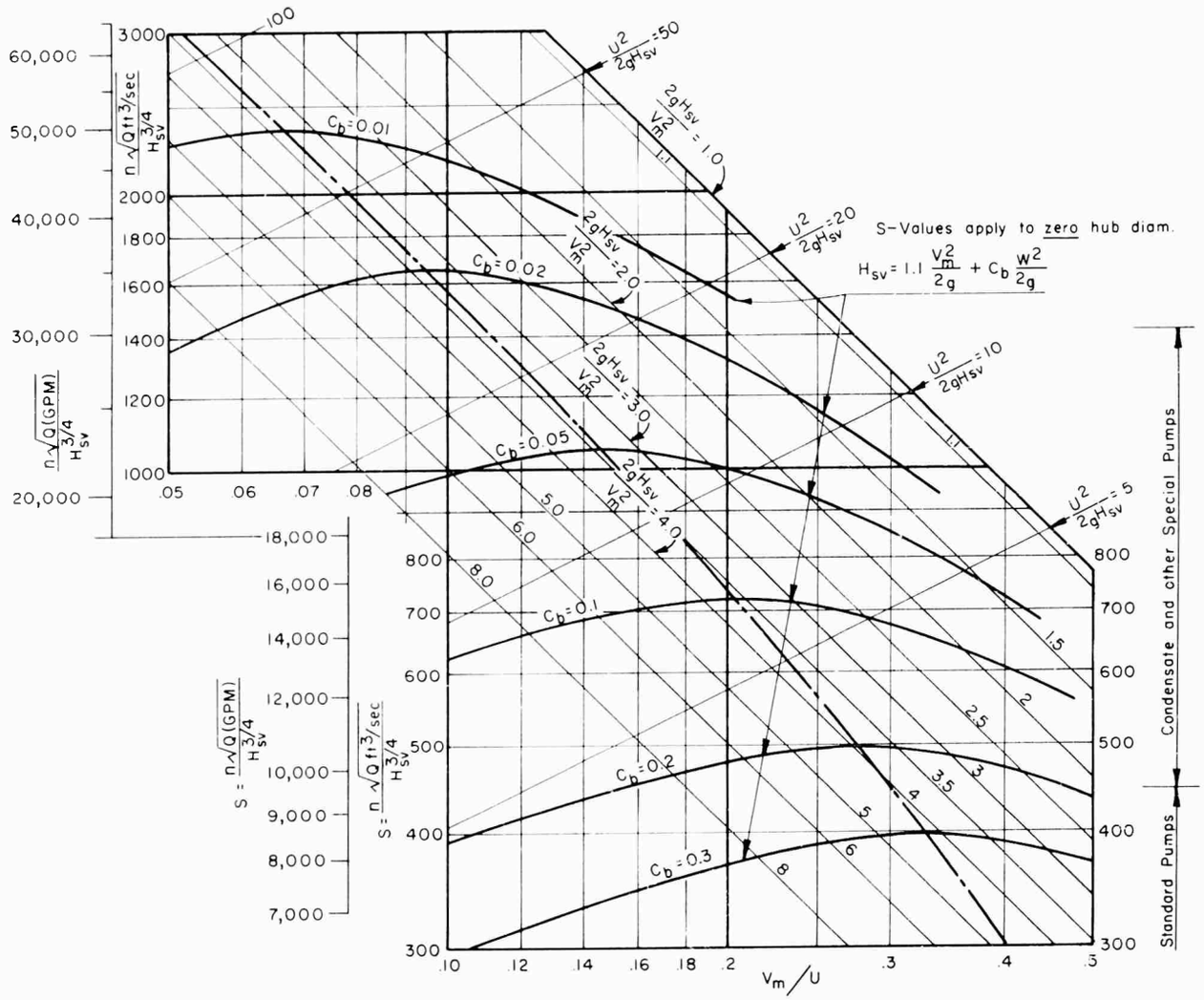

Fig. 13 - Relationship of the Cavitation Parameters of Turbomachinery

be of greater interest to refer the speed of rotation to the thrust and forward velocity of the propulsor, which are the primary performance characteristics of a pumpjet. These quantities can be used to derive a "propulsor specific speed":

$$n_{P_S} = \frac{n\sqrt{F}}{V^2}\ , \qquad 26$$

which may be defined (quite analogously to the specific speed) as, "that combination of thrust, forward velocity, and speed of rotation that, if maintained constant, permits similar flow conditions in geometrically similar pumpjets or any other type of rotating propulsor." Thus, all propulsors that have (for the same mass density of the fluid) the same value of the propulsor specific speed (n_{P_S}), can be (but do not have to be) geometrically similar; i.e., they can be derived from each other by a simple process of scaling and by changes in absolute velocity and speed of rotation.

The value of this similarity criterion of rotating propulsors is not likely to become apparent before this coefficient has been calculated for a large number of propulsors, and the various design and flow characteristics of the propulsors have been plotted as a function of the propulsor specific speed. The foregoing use of pump characteristics has, at present, the advantage that these characteristics have been used successfully.

F. Over-All Design of a Pumpjet Operating on the After End of a Body of Revolution

This section of the report covers the over-all design of a pumpjet located on the trailing end of a propelled body of revolution as shown in Fig. 14. The arrangement is quite similar to that discussed in reference 7.

AVERAGE VELOCITIES

Since the inlet of such a pumpjet is exposed to the boundary-layer flow of the propelled body, the inlet velocity V_1 is obviously not uniform with respect to the distance from the body. A first approximation for the design of the passages within the pumpjet shroud can be obtained by considering average meridional velocities ($\overline{V}$) By the use of such average velocities, considerations are obviously quite similar to those given in Section D; however, the definitions of average velocities under the conditions described here require some consideration.

An average of the meridional through-flow velocity may obviously be defined using the condition of continuity:

$$\overline{V} = \frac{1}{\Delta y}\int_0^{\Delta y} V\, dy, \qquad 27$$

where Δy is the thickness of the flow layer taken into the pumpjet measured normal to the direction of the flow. However, if the momentum of the flow is being considered, the definition of an average velocity is

$$\overline{V} = \int_0^{\Delta y} V^2 dy \Big/ \int_0^{\Delta y} y\, dy \qquad 28$$

If the energy transport through the cross section is to be evaluated, the corresponding average velocity would be defined by

$$\overline{V}^2 = \int_0^{\Delta y} V^3 dy \Big/ \int_0^{\Delta y} y\, dy \qquad 29$$

Fortunately, the differences in average values defined according to equations 27, 28, and 29 are not very large; and it is probably sufficient to use only one of these definitions in all cases. The definition given by equation 28 with respect to the momentum of the meridional flow represents a usable mean value.

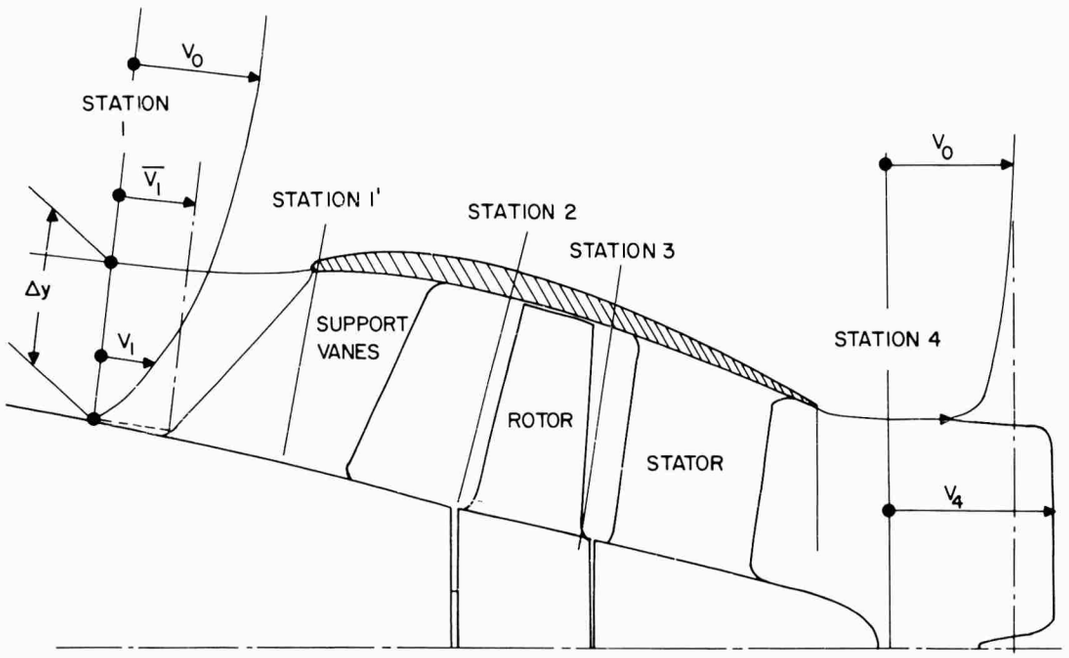

Fig. 14 - General Arrangement of a Pumpjet Located at the After End of a Propelled Body of Revolution

VELOCITY PROFILES AHEAD OF THE SHROUD

The velocity distribution over the boundary layer of a body of revolution is rarely given by theoretical considerations; it is determined by a wake survey, usually taken in a plane midway between the leading and trailing edges of the propeller or pumpjet rotor that replaces the propeller. This measured velocity distribution may then be transferred to another cross section, such as a cross section ahead of the pumpjet inlet, either by assuming the total energy of the flow to be constant along streamlines or by using the laws of vortex flow through turbomachinery (11). These laws become identical with the foregoing conditions if the assumption is made that the propulsor imparts a constant amount of energy per pound of fluid along every streamline of the flow through the rotor.

In reference 11, the general relationship for vortex flow through turbomachinery (under axially symmetrical flow conditions) is shown to be

$$\frac{\vec{\zeta} \times \vec{V}}{\rho R V_m} = \text{constant} \qquad 30$$

along streamlines. As long as the vorticity vector $\vec{\zeta}$ is normal to the velocity of flow, which is true in the boundary-layer flow ahead of the pumpjet vane systems, equation 30 can be simplified to

$$\left(\frac{\partial V_m}{\partial n} + \frac{V_m}{r}\right)\frac{1}{R} = \text{constant}, \qquad 31$$

where r is the radius of curvature of the meridional streamlines, n is the coordinate normal to the streamlines (previously referred to as y), and R is the distance from the axis of rotation. Equation 31 is valid throughout the pumpjet if all vane systems have radially or spanwise uniform circulation; it is always valid along a streamline as long as $\vec{\zeta}$ is normal to $\vec{V}$.

Equation 1 and the considerations used in Section D are directly applicable with respect to the average through-flow velocity on the end of a body of revolution if it can be assumed that the static pressure some distance ahead of the pumpjet inlet and some distance behind its discharge is equal to the free-stream pressure p_0. This assumption is reasonably close, because the static pressure on the surface of a body of revolution passes through the value of the free-stream pressure near the after end of the body, as shown in Fig. 15. Thus, the assumption of equal static pressures ahead of the inlet and behind the discharge of such a pumpjet may be used as an approximation. Generally the true velocities and pressures should be used, and they can be determined either theoretically or experimentally.

SHROUD DESIGN

The pumpjet shroud may now be designed in a manner similar to that described in Section D and Fig. 6. The configuration of a pumpjet on the end of a body of revolution is shown in Fig. 16, where the angle of attack α is to be used in the manner described in Section D. This angle should, therefore, be limited to values near 15 deg. Equation 22 may be used to obtain an additional check on the lift coefficient of the shroud, although it should be remembered that equation 22 applies primarily to flow conditions without the action of a rotor within the shroud.

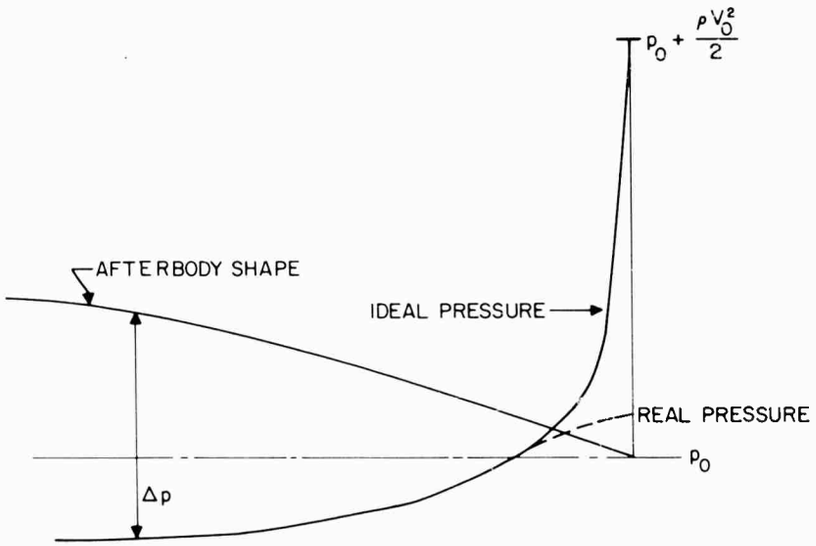

Fig. 15 - Pressure Distribution over the After End of a Body of Revolution

The lift coefficient of the shroud may also be calculated as suggested in reference 7, but it must be remembered that all suggested approximations are incomplete with respect to one of the most important aspects of shroud design: separation of the flow from the external surface of the shroud. Such separation obviously could occur with a shroud of zero lift coefficient in connection with a conical afterbody having a rather steep angle of convergence. The over-all problem of shroud design must therefore be considered as still unsolved.

VELOCITY PROFILES WITHIN THE SHROUD

Actual results of velocity calculations for the flow inside a pumpjet shroud, as described above, are shown in Fig. 17 for four stations within the shroud and a station at the discharge end of the shroud. The velocity distributions for stations 2, 3, 4, 5, and 6 are derived from the bare-body velocity distribution (shown in the figure) on the basis of equation 31. It should be evident

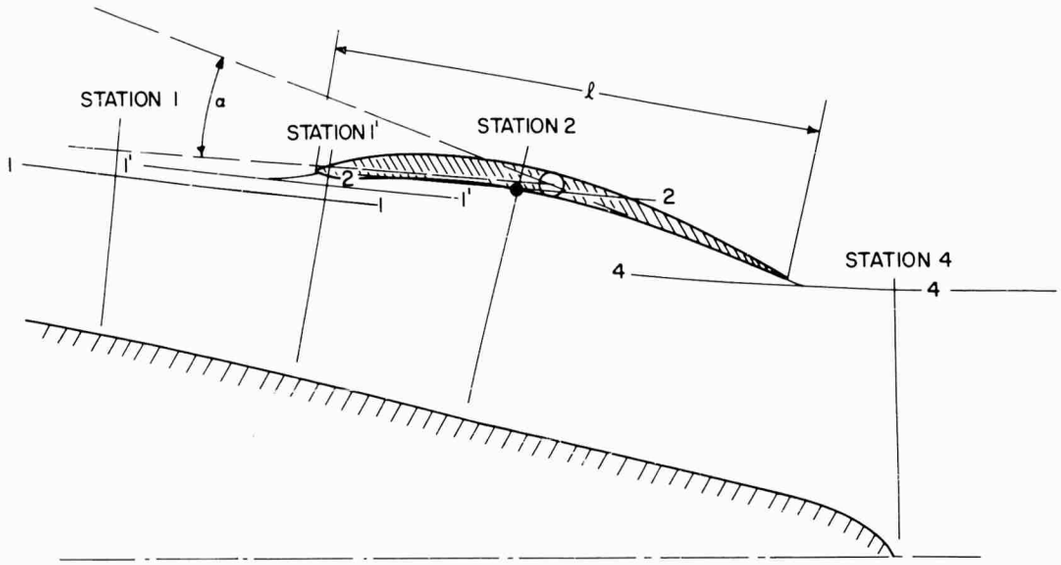

Fig. 16 - Pumpjet Shroud on Tapered Afterbody

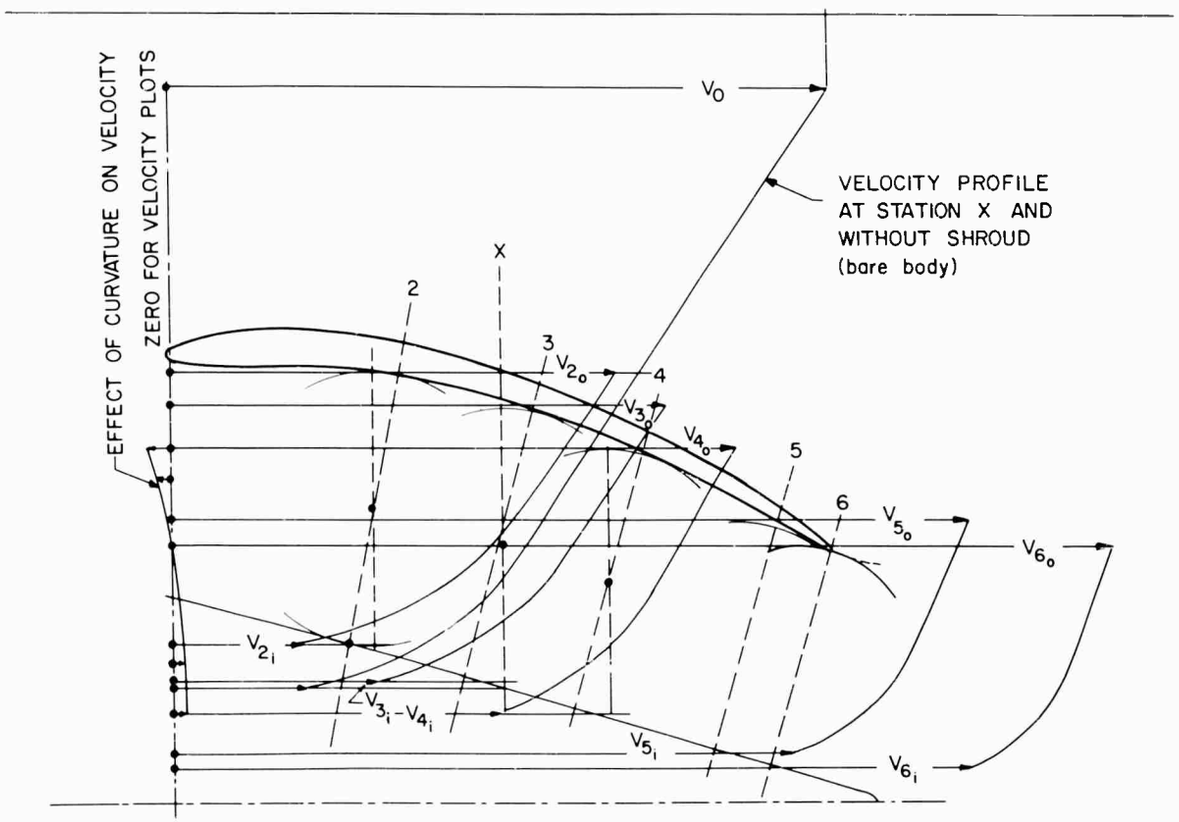

Fig. 17 - Velocity Distribution within a Shroud on a Tapered Afterbody

that this solution can be obtained only by a process of successive approximations that must satisfy the condition of continuity for the flow cross section inside the shroud. The effect of curvature on the flow, as expressed by the second term in equation 31, can be approximated separately as shown by the curve so indicated in Fig. 17. This curve is constructed as described in Section D and Fig. 7. For a pumpjet mounted on a conical afterbody, the same process is illustrated in Fig. 18. The velocity variations ΔV_R produced by the curvature of the flow may be algebraically added to the velocities derived for zero curvature. Figure 17 shows that curvature has very little effect on the flow inside the shroud.

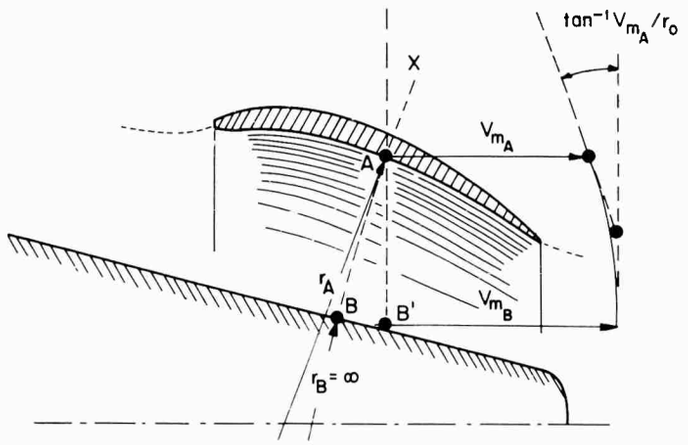

Fig. 18 - Effects of Curvature on Flow Characteristics within a Shroud

FRICTIONAL EFFECT

The foregoing derivation for the meridional flow inside the shroud is based on the assumption of frictionless flow. Actually, a boundary layer is formed on the inside of the shroud and along the central body. It is usually not practical to attempt an estimate of these frictional effects; they are exceedingly difficult to predict because of the influence of the vane systems both ahead of and within the shroud. Instead, it is suggested that stations 2, 3, 4, 5, and 6 (Fig. 17) be corrected for an estimated thickness of the boundary-layer-displacement thickness on the walls of the annular passage. If there is a retardation between the inlet and station 2, a fairly rapid growth of the boundary-layer-displacement thickness is to be expected - perhaps amounting to about 10 per cent of the total cross section. A similar addition in cross-sectional area may be justified for stations 3 and 4. At stations 5 and 6, however, a smaller increase should be used because of the acceleration of the meridional flow from station 4 to station 6. The suggested increases in flow areas beyond those required for the theoretically obtained velocities are empirical, and they should be adjusted according to experimental results obtained with the actual propulsor.

G. Design of Pumpjet Rotor Blades

DESIGN SURFACES

After determining the velocity distributions in the space between the shroud and the central body, it is possible to derive streamlines of the flow in this region on the basis of the simple relationship

$$V_m \, \Delta a = \text{constant}, \qquad 32$$

where $\Delta a = R \Delta n 2r$, in which Δn is the distance between streamlines (measured normal to the streamlines) and R is the radial distance from the axis of symmetry.

The meridional stream surfaces so determined are generally not axial. It is entirely possible to treat the flow through a vane system along these more-or-less conical stream surfaces; however, the empirical data developed in connection with the axial-flow-compressor developments mentioned in Section A apply primarily to straight, cylindrical stream surfaces. Furthermore, the theoretical treatment of the flow along straight, cylindrical stream surfaces is far simpler than that of the flow along concial stream surfaces because, in the latter case, the flow relative to rotating vanes has an inherent vorticity associated with the rotation of the blades. Thus, the theoretical treatment of the flow is substantially complicated.

To apply cascade data - particularly those developed by NACA for stright axial flow through this type of vane system - and to avoid the theoretical complications of the flow along conical surfaces, the present design procedure determines the blade shape by considering only the axial component of the meridional flow through the vane system. Thus, as shown in Fig. 19, the flow is examined on the basis of a straight cylindrical section A-A. The meridional velocity of the flow entering the vane system is determined by the preceding considerations for the stream surface b-b; and the inlet velocity to the vane system along section A-A is simply the axial component of the meridional velocity along b-b at the inlet edge of the system. For the discharge of the vane system, the meridional velocity is that determined previously for the stream surface a-a; the discharge velocity along the cylindrical section A-A is simply the axial component of the meridional velocity along a-a at the point where this stream surface intersects the trailing edges of the vane system. The axial velocity along the cylindrical surface A-A will change between inlet and discharge, not only because of changes in the cross section of the meridional flow but also because the flow passes from one meridional stream surface to another.

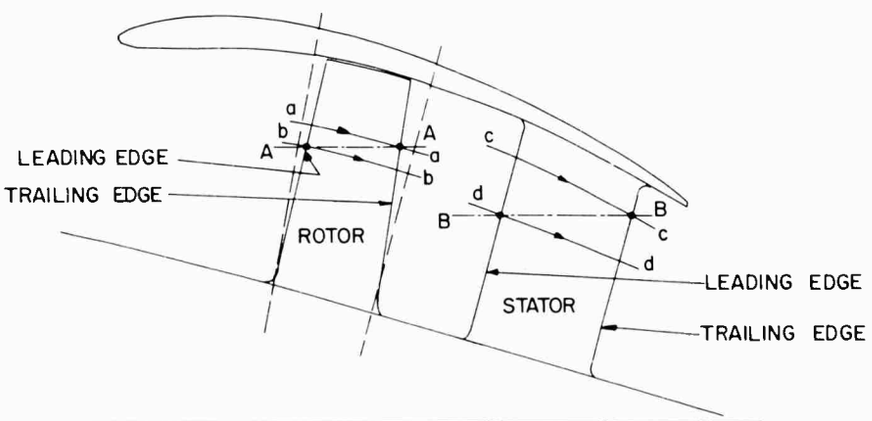

Fig. 19 - Flow Surface in Meridional Plane

The actual meridional flow consists of the flow along the cylindrical stream surface A-A plus a spanwise flow that changes the cylindrical flow to the flow along the more-or-less conical stream surfaces a-a and b-b. As long as the vane circulation does not change in the spanwise direction, it is reasonable to neglect this spanwise component of the meridional flow. The design method presented here is based on such an assumption.

In reality, the flow problem involved is somewhat more complicated. The spanwise flow can be neglected only if spanwise blade sections happen to have the same direction as a spanwise flow of constant angular momentum. Actually, spanwise sections (called fairing sections) of the vanes will be determined largely by the geometric considerations described at the end of this section. Usually, a spanwise flow of constant angular momentum does not occur; however, the situation is not violated in principle if the leading edge of the vanes falls approximately within a radial plane and if the incoming flow has no circumferential component. It should be recognized that the procedure (based on neglecting the spanwise component of the meridional flow) is not exact, and this problem deserves further critical examination.

THE MEAN STREAMLINE

The blade profiles along cylindrical sections, such as A-A of Fig. 19, can be designed by several methods. The method used here is the "mean-streamline" method, which is described in reference 10. This method determines changes in the circumferential component of the flow through the vane system caused by the pressure differences along the blade and the departure of the blade camber line from the mean streamline so determined by a semiempirical analysis of NACA cascade data based on the same mean-streamline principle. An example of a blade layout for a fairly large ratio of axial to circumferential relative-velocity component is shown in Appendix A. (The Appendix consists of four actual blade designs.) The inlet velocity vector of the relative flow (w_2) and the discharge velocity vector of the relative flow (w_3) are determined by: (a) the axial components of the meridional flow at inlet and discharge; (b) the peripheral velocity of the blade at the cylindrical stream surface A-A; and (c) the change in circumferential component of the flow (ΔV_u), which is determined by the Euler equation of turbomachinery (equation 6). The subscripts 2 and 3 denote the stations ahead of and behind the rotor (see Fig. 1).

The axial component of the discharge relative velocity (w_3) is not exactly equal to that determined by the flow shown in Fig. 17. It is larger by an amount equal to the area reduction produced by the blade thickness at the discharge edge plus the displacement thicknesses of both blade boundary layers leaving the blade profile. Appendix A shows a typical curve along which the ends of the relative velocity vectors travel from the inlet to the discharge. It is difficult to determine the exact displacement thickness of these boundary layers; however, the reduction in meridional cross section caused by the blade boundary layers can be estimated and an appropriate increase (greater than that given by Fig. 17) can be made in the axial component of w_3. The axial component of the relative velocity at intermediate locations between the inlet and discharge of the rotor can be obtained in exactly the same manner.

The circumferential component of the absolute velocity at intermediate locations is determined by a simple proportion of the diagram of blade pressure vs axial length. The circumferential component of the relative velocity can then be obtained by subtracting the blade speed from the circumferential component of the absolute velocity. Details of this procedure are given in reference 10.

The mean streamline may now be drawn by the so-called "method of isoclines"; i.e., it is constructed such that it is tangent to the relative velocity vector at every point.

THE MEAN CAMBER LINE

The departure of the mean camber line of the blade from the mean streamline is assumed to be proportional to the lift coefficient of the blade. The distribution of this departure along the blade profile is derived from NACA cascade data, as described in reference 10. A typical departure curve suitable for vane systems requiring high resistance to cavitation is shown in Fig. 20. The unit of departure is the maximum departure of the standard NACA 65-series cascades as shown in Fig. 21 (from reference 10).

The lift coefficient of the blade is most easily determined by equation 265 of reference 10. The equation, rewritten with the notations used in this report, is

$$C_{L_\infty} = 2 \frac{\Delta V_u}{w_\infty} \frac{t}{l} , \qquad 33$$

where t is the circumferential spacing of the vanes, l is the chord length of the blade, and w_∞ is the vectorial mean between the relative inlet and discharge vectors.

If the lift coefficient is referred, instead, to the inlet relative velocity,

$$C_{L_2} = C_{L_\infty} \frac{w_\infty^2}{w_2^2} . \qquad 34$$

The value of C_{L_2} can also be determined from the mean pressure difference across the blades as derived from the assumed pressure-distribution diagram shown in Appendix A. It is seen that

this diagram uses $\rho w^2/2$ as the difference between the free-stream pressure and the stagnation pressure; therefore,

$$C_{L_2} = \frac{2}{\rho w_2^2} \int_0^{l_a} \Delta p \, dl'_a \, \frac{1}{l_a} \, , \qquad 35$$

where Δp is the pressure difference as plotted in the pressure-distribution diagram, l'_a is the coordinate of the blade in the axial direction, and l_a is the total axial extent of the blade.

Equations 33, 34, and 35 relate the velocity diagram to the pressure changes and the so-called "solidity" of the vane system (l/t).

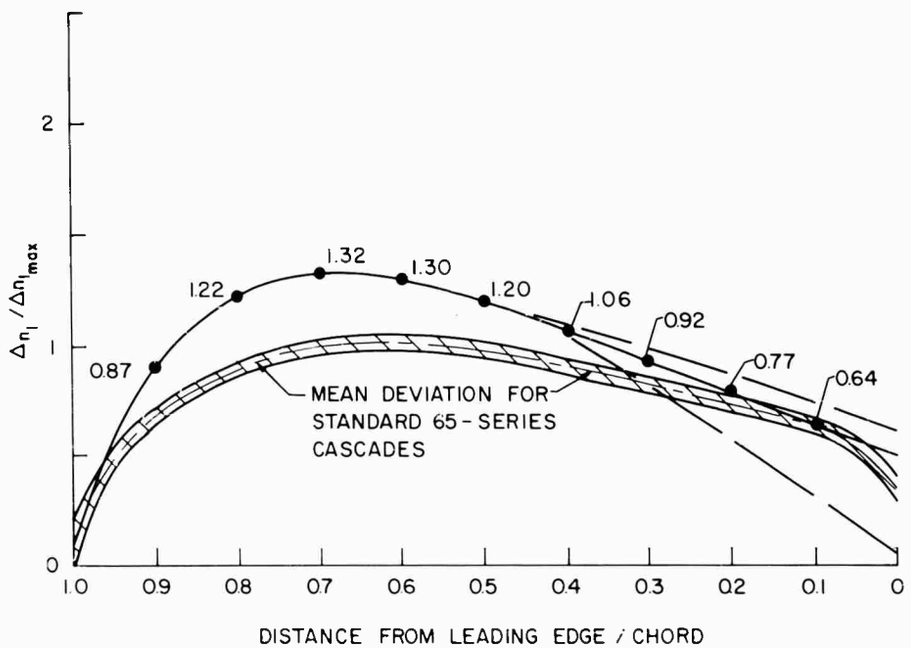

Fig. 20 - Chordwise Distribution of Camber-Line Offsets

The maximum departures of the camber line of the blade from the mean streamline are plotted in Fig. 21 as a function of the so-called "stagger" angle of the vane system (β) measured, in this case, from the axial direction of the vane system. The departure Δn_l is measured normal to the base or chord line of the blade and is referred, in Fig. 21, to the unit lift coefficient. Figure 21 represents these departures for the standard 65-series cascades investigaged by NACA.

Figure 20 shows the distribution of the camber-line departure from the mean streamline along the length of the blade. The solid curve shows departures derived from so-called "trailing-edge loaded" profiles investigaged by NACA. In this case, the maximum departure is larger than unity; i.e., it is larger than the maximum departure of the standard NACA 65-series profiles. The mean departure curve for the standard 65-series is also shown for comparison.

The actual departure is determined from those shown in Fig. 20 by the relationship

$$\Delta n = \left(\frac{\Delta n_l}{l}\right)_{max} \left(\frac{\Delta n_l}{\Delta n_{l_{max}}}\right) C_{L_\infty} \, l \, , \qquad 36$$

where $\Delta n_l / \Delta n_{l_{max}}$ is the value read directly from Fig. 20 for the various stations along the chord of the blade. On the horizontal axis of this figure, 0 indicates the leading edge and 1 indicates the trailing edge of the blade.

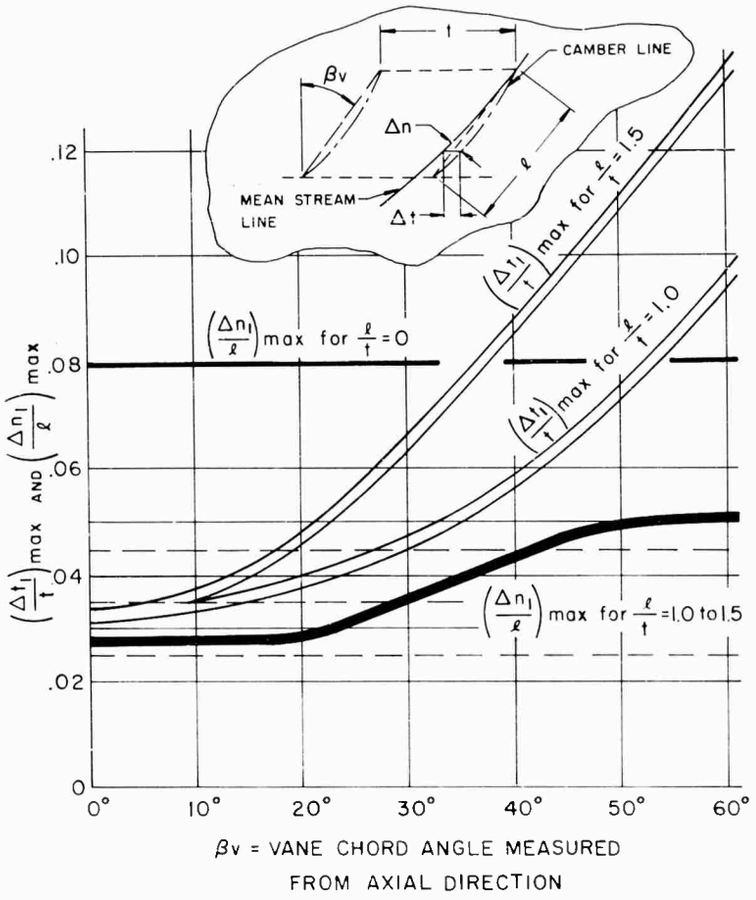

Fig. 21 - Unit Camber-Line Departure for NACA 65-Series Cascades

After determining the camber line of the blade in this manner, the thickness of the blade is determined from the changes in the axial component of the relative flow by the relationship

$$\frac{\tau}{i} = \frac{\Delta V_a}{V_a} \quad , \tag{37}$$

where τ is the circumferential blade thickness. The originally assumed curves along which the relative velocity vectors travel from the inlet to the discharge will not produce a profile that has a smooth contour; therefore, it is generally necessary to correct the contour to obtain a hydrodynamically acceptable shape. To meet the over-all conditions, this contour is drawn with a minimum of curvature along the sides of the blades; the resulting profile is generally a decisive factor in blade performance.

DESIGN EXAMPLES

From the departure curve in Fig. 20, it will be noted that a variation of this curve is indicated near the leading edge because the action of the blade is largely determined by its trailing portion. The manner by which this freedom of choice for the departure curve near the leading edge can be utilized to meet flow conditions is discussed in the following examples of blade design.

Appendix B shows the blade profile for the tip section of a pumpjet rotor of a much lower advance ratio than that shown in Appendix A; however, the principles of design are exactly the same.

Appendix C shows a blade profile, also derived by the same method as that in Appendix B, for the root section of a pumpjet rotor of fairly low advance ratio. The required flow deflection for this root section is, of course, much greater than that of the tip section of such a rotor (Appendix B), because the change in circumferential component multiplied by the peripheral velocity of the particular section must remain constant, as indicated by equation 6.

THE LEADING EDGE

Appendix C shows a consideration that limits the choice of the blade shape near its leading edge, which was left somewhat undetermined by the departure curves in Fig. 20. The length δ is established by drawing a line perpendicular to a line through the leading edge that has the direction of the incoming flow and such that it passes through the leading edge of the neighboring blade. This distance δ should not be obstructed by any portion of a blade; otherwise, the flow in the region ahead of the vane system would have to be accelerated between the vanes. It should also be clear that this distance is strongly influenced by the choice of the departure curves near the leading portion of the blades. For the tip sections, where the blades do not usually overlap, the lower departure curve shown in Fig. 20 can be used. For root sections, such as that shown in Appendix C, it may be necessary to use the upper departure curve to make certain that the distance between the blades does not require an acceleration of the mean flow when entering the blade system.

FLOW SEPARATION

For strong deflections, such as those that occur in the root sections (Appendix C), it is necessary to consider limits of retardation as determined by separation of flow from the low-pressure side of the blades ("stall"). Considerations with respect to stall are discussed in reference 10. As a simple rule of thumb, it should be considered that the relative discharge velocity of the system should be preferably not less than 0.6 of the relative inlet velocity but never less than half that velocity. The velocity condition shown in Appendix C represents very nearly a limiting case of retardation of the relative flow between the vanes.

STATOR BLADES

The same design considerations described for the rotor vanes also apply to the stator vanes behind the rotor. Again, the more-or-less conical meridional streamlines are replaced by a cylindrical section B-B, as shown in Fig. 19. A typical diffuser vane section derived by the mean-streamline method is shown in Appendix D. If the shroud is properly designed, the meridional component of the flow (and thereby the axial component of the flow in the blade section) can be sufficiently accelerated to avoid any retardation of the flow within the diffuser-vane system. As a result, boundary-layer growth and corresponding losses within the vane system should be minimized. This design expediency is obviously not available for standard axial-flow pumps, because an acceleration of the meridional flow would result in losses in the discharge passages of the pump.

FINAL BLADE DESIGN

The design of the individual vane sections on the basis of local flow conditions is incomplete in at least two respects: (a) the relationship between the velocities, the pressures, the solidity (t/ℓ), and the lift coefficient as expressed by equations 33, 34, and 35, leaves considerable freedom of choice with respect to the variables involved; and (b) the pressure difference across the blade (ΔP) - as

shown, for example, in Appendix A - should be determined in a manner such that a given, reasonably uniform, cavitation performance is obtained. For the blade section considered in Appendix A, it is seen that the pressure reduction below the mean static pressure at the inlet is $0.29\ (\rho w_2^2/2)$, where w_2 is the relative inlet velocity. For the particular example considered, it is seen that $w_2 = 1.429\ V_\infty$. Therefore, if the static-pressure difference between the rotor inlet and the free stream is neglected, the cavitation number referred to the forward velocity of the propelled body (V_∞ or V_0) is

$$\sigma = 0.29\ \frac{V_0^2}{w_2^2} = 0.29 \times 1.429^2 = 0.59. \qquad 38$$

In reality, the cavitation number is likely to be somewhat greater, because the pressure distribution cannot be expected to be exactly that shown in Appendix A.

The pressure distributions may now be selected for other blade sections so that the cavitation number (σ) is about the same for all blade sections. The inner blade sections are usually designed for a slightly lower cavitation number than that determined by the foregoing considerations so that the possibility of cavitation is greatest at the tip - where the deflection of the flow is a minimum - and agreement with the approximation used here might be an optimum.

After determining the pressure reduction, and thereby - to some extent - the average pressure difference over the blade from cavitation considerations, an approximation is obtained for the lift coefficient on the basis of equation 35, and the appropriate values of the solidity (t/ℓ) of the various sections may be determined.

The cascade sections obtained are dimensionless and must first be adjusted so that the blade spacing (t) varies with the distance from the axis and yields a whole number for the number of blades. The absolute size of the blades or their aspect ratio is still undetermined; i.e., the same geometric form can be obtained for the various cascade sections with various numbers of blades. The actual number of blades or the actual aspect ratio must be determined by considering the bending stress and, if possible, the elastic bending deformations in the final blades.

Even this consideration does not necessarily produce a satisfactory answer, because the overall geometry of the blade may, as yet, be unsatisfactory. It is necessary to "stack" the blades, i.e., inspect the cylindrical sections after they are placed one on top of the other (see reference 10). It is evident that a truly satisfactory blade design can be obtained only by a series of successive approximations.

H. A Small, High-Speed Pumpjet with Boundary-Layer Intake

THE USE OF A HIGH-SPEED PUMPJET TO REDUCE MACHINERY WEIGHT

Thus far, only pumpjets with speed and size characteristics similar to those of standard propellers have been considered. However, a small, high-speed pumpjet with an intake submerged deeply in the boundary layer of the vehicle that it propels has certain advantages. Such a propulsor is discussed thoroughly in reference 9. The substance of that discussion is that a high rotational speed implies a reduction in the weight of the power-transmitting machinery (because of the lower torque involved) and perhaps the elimination of the speed-reducing gears. The weight reduction can be utilized either to carry larger payloads or to attain higher vehicle speeds. However, to obtain higher rotational speeds, a smaller rotor diameter is required thereby reducing the flow rate through the pumpjet. Low flow rates, in turn, imply a low propulsive efficiency (as discussed in Section B) and, hence, require a larger power plant, which can offset the anticipated weight reduction. Some of this loss in propulsive efficiency can be regained by submerging the inlet of the propulsor deep in the boundary layer of the vehicle. As a result, the inlet velocity is reduced and the propulsive efficiency is increased (see reference 9).

ANTICIPATED SPEED INCREASES

The magnitude of the possible speed increase that can be obtained in such a propulsor is demonstrated by the following analysis. Although this approach applies to both pumpjets and

propellers, the boundary-layer-intake idea is more characteristic of pumpjets than propellers because the presence of a shroud gives the designer much more control of the flow into the propulsor.

Equation 12 may be written:

$$\Delta\left[\frac{V_u}{U}\,\frac{U^2}{V_0^2}\right] = \frac{1}{2\eta_H}\,\frac{C_D}{m_0}\left(\frac{d_0}{d_P}\right)^2\frac{V_0}{V_1}\left[\frac{1}{4}\,\frac{C_D}{m_0}\left(\frac{d_0}{d_P}\right)^2\frac{V_0}{V_1}+2\,\frac{V_1}{V_0}\right], \tag{39}$$

where d_0 is the maximum diameter of the propelled vehicle, d_P is the rotor tip diameter, and m_0 is a fictitious flow rate defined as

$$m_0 = \frac{Q}{\frac{\pi}{4}V_1^2\,d_P^2}\,. \tag{40}$$

It should be noted that m_0 is essentially constant, which is equivalent to assuming that the flow rate varies as $V_1{}^2d_P{}^2$ (a reasonable assumption). The quantity $\Delta(V_u/U)$ is proportional to the pressure coefficient of the rotor, which should be kept as high as present practice will allow; therefore, $\Delta(V_u/U)$ should be considered a constant. Thus, it can be deduced from equation 39 that $U^2/V_0{}^2$ varies at least as $1/d_P{}^2$, and that such a variation is a conservative estimate because of the added dependence on V_1, which also must decrease with decreasing dP.

AN EXAMPLE

An exact prediction of the variation in $U^2/V_0{}^2$ with propulsor diameter d_P is, therefore, dependent upon the type of application. It must be pointed out, however, that V_1 decreases slowly with decreasing propulsor diameter; therefore, it produces only a slight effect on the quantity $U^2/V_0{}^2$. Because U is proportional to the rotational speed, n, of the propulsor (at the tip $U = \pi\, nd_P$), an estimate of the variation of n with d_P can be made to demonstrate this principle; consider the following example.

Submarine propellers are relatively smaller than torpedo propellers (submarines ordinarily operate with a d_P/d_0 ratio of approximately 0.5; for torpedoes this ratio is approximately 0.86). Thus, the propulsive efficiencies of submarines are somewhat lower than those of torpedoes. It would be of interest to determine what reduction in torpedo propeller diameter and, hence, what increase in rotational speed could be obtained by reducing the propulsive efficiency to that of the submarine.

The first step is to write equation 5 in the following manner:

$$\eta_P = \frac{1}{\frac{1}{4}\,\frac{V_0}{V_1}\,\frac{C_D}{m_0}\,\frac{d_0^2}{d_P^2}+\frac{V_1}{V_0}} \tag{41}$$

But, if the propulsive efficiency of the torpedo is to equal that of the submarine

$$\left[\frac{1}{\frac{1}{4}\,\frac{V_0}{V_1}\,\frac{C_D}{m_0}\,\frac{d_0^2}{d_P^2}+\frac{V_1}{V_0}}\right]_{\text{torpedo}} = \left[\frac{1}{\frac{1}{4}\,\frac{V_0}{V_1}\,\frac{C_D}{m_0}\,\frac{d_0^2}{d_P^2}+\frac{V_1}{V_0}}\right]_{\text{submarine}}.$$

However, assuming that V_1/V_0 is very nearly equal to 1.0 in both cases (a conservative assumption since both propellers, and especially the submarine propeller, operate in the boundary layer of the body), and since m_0 is very nearly a constant for both vehicles, then

$$\left[C_D\,\frac{d_0^2}{d_P^2}\right]_{\text{torpedo}} = \left[C_D\,\frac{d_0^2}{d_P^2}\right]_{\text{submarine}} \tag{42}$$

The drag coefficient, C_D, is approximately 0.07 for submarines and 0.11 for torpedoes, whereas d_P/d_0 for submarines is about 0.5. Thus, the rotor-to-body-diameter ratio of a torpedo operating at the same propulsive efficiency as that of a submarine would be

$$\left(\frac{d_P}{d_0}\right)_{torpedo} = 0.5\sqrt{\frac{0.11}{0.07}} = 0.627$$

as compared to the normal value of 0.86. If the above variation of the peripheral velocity squared with $1/d_P{}^2$ is now used (which has been shown to be conservative), the resulting rotational speed is greater by a factor of 1.9. Thus, the rotational speed of the torpedo propeller could be almost doubled yet could maintain the same propulsive efficiencies as those of submarines.

This increase in shaft speed by a factor of 1.9 is still too low to result in any drastic simplifications; however, further increases can be obtained by employing a boundary-layer intake. In reference 9, which contains a complete discussion of boundary-layer intakes, it is assumed that 75 per cent of the total drag occurs ahead of the propulsor. This is sufficient information for calculating the boundary-layer profile, and the propulsive efficiency can be determined as a function of the percentage of the boundary layer inducted into the propulsor. Figure 7 of reference 9 shows this function and indicates that a propulsive efficiency of better than 80 per cent can be obtained by inducting 20 per cent of the boundary layer, whereas the propulsive efficiency drops off rather rapidly as lower percentages are inducted. The torpedo pumpjet that will be described here was designed using this 20 per cent criterion, and it resulted in a d_P/d_0 ratio of 0.31 as compared to the more normal value of 0.86. Using the $1/d_P{}^2$ rotational speed variation, propulsor rotational speeds can be obtained that are about 7.5 times greater than those normally employed by torpedoes. Thus, it is possible to obtain speed increases that are large enough to result in significant simplifications and still maintain acceptable propulsive efficiencies.

This result can be applied in equation 42 to determine what rotational speed increases might be possible for a submarine propelled by a pumpjet with boundary-layer intake while maintaining acceptable propulsive efficiencies. Thus,

$$\left(\frac{d_P}{d_0}\right)_{submarine} = 0.31\sqrt{\frac{0.07}{0.11}} = 0.247$$

as compared to the more normal value of 0.5. Again, using the $1/d_P{}^2$ variation, submarine rotational speeds could be increased by a factor of 4.1 by the use of a boundary-layer intake and could still maintain acceptable propulsive efficiencies.

While discussing this subject of machinery weight reduction it should also be pointed out that an additional reduction is possible for propulsors operating in series. This additional reduction can be obtained by multistaging, and is a simple application of the square-cube law. The strength of a shaft is proportional to the square of its diameter, whereas the weight is proportional to the cube of the diameter; hence, the additional weight reduction is obvious.

I. External Design of a High-Speed Pumpjet with Boundary-Layer Intake

LOW-DRAG BODIES

A body with a large diameter-to-length ratio (d_0/L) has better drag characteristics than a body with a smaller diameter-to-length ratio because the former has a smaller surface-area-to-volume ratio. However, separation of the boundary layer over the after portion of such a body results in large form drag that can prevent the designer from taking advantage of the inherently low skin-

friction drag. The high-speed pumpjet with boundary-layer intake can act as a boundary-layer suction device to eliminate this separation and the associated high form drag. Therefore, when a conventional propulsion system is replaced with a small, high-speed pumpjet that has a boundary-layer intake, the original body can also be replaced with one of a larger d_0/L ratio and thus offset the reduced efficiency of the high-speed pumpjet with the reduced drag of the body with the larger d_0/L ratio.

For such a combination, the location of the inlet is dictated by the shape of the body rather than by the pumpjet characteristics. Usually the inlet will be located a considerable distance forward on the body, and the pumpjet shroud will be quite long. The control surfaces can be located on the shroud and thereby eliminate any direct interaction between the control surfaces and the pumpjet. Of course, the outside surface of the shroud must be carefully designed, or separation will occur on it; in fact, the outside surface of the shroud is probably the most critical part of the design. The exit jet has a favorable effect on the shroud performance because it tends to "draw" the fluid over the shroud and thus prevent separation. Although every shroud observed by the authors exhibited flow separation without the pumpjet running, flow separation did not occur on the carefully designed shrouds when the pumpjet was running. Figure 22 shows a pumpjet in a moving stream with the rotor at rest. Flow separation on the outer surface of the shroud is disclosed by the motion of the tufts. Figure 23 shows the same pumpjet but with the rotor operating; no flow separation is evident. This pumpjet, which is a small, high-speed unit with a boundary-layer intake, was designed for a torpedo-shaped body. For this particular design, no attempt was made to take advantage of the higher vehicle d_0/L ratios possible with such a propulsor. The pumpjet was designed to take in 20 per cent of the total boundary layer (as discussed in the previous section). This shroud will be used as an example of a method for designing the outside contour of a type of shroud that would be used with bodies having a high diameter-to-length ratio.

SHROUD DESIGN

The possibility of separation on a surface is minimized by shaping the surface so that the adverse pressure gradient along its length is as gradual as possible. For the shroud of the boundary-layer-intake pumpjet discussed here, this can be done by determining the streamlines over bodies of revolution of various shapes and determining the pressure along a streamline that is located approximately where the shroud must be located for each of the bodies investigated. Then, the streamline having the most gradual pressure gradient is chosen, and this streamline is used for the outside shape of the shroud. This procedure will now be described in more detail.

The flow over a body of revolution can be determined by the combintaion of a source (or sink) and a uniform flow. The strength of the source (or sink) is chosen so that the diameter of the body formed by the closed streamline (i.e., the diameter infinitely far from the source, or sink) is the same as the body in question. For this particular design, the streamlines of such a flow were determined by a graphical method that is probably the quickest way of finding a solution. The closed streamline was first determined; a second streamline was then located normal to the body and at a distance from the first streamline equivalent to 20 per cent of the boundary-layer thickness. The pressure variation along this streamline was determined and found to be too drastic; therefore, a second representation of the body was used that consisted of two sinks and a uniform flow, and the streamline pattern was again determined graphically. The resulting streamline pattern is shown in Fig. 24. The velocities along the streamline that correspond to 20 per cent of the boundary-layer thickness (and, hence, the pressures) are indicated and, as can be seen, the variation is quite gradual. Therefore, the outside surface of the shroud was made to correspond, as nearly as possible, to the contour of this streamline.

Figure 25 shows the final shape of the shroud with the streamlines from Fig. 24 superimposed. The external contour of the shroud is seen to correspond quite well to the streamline except near the discharge where it must deviate to produce the proper jet diameter. It is in this area that the jet-pump action must prevent separation.

From the actual performance of this shroud (Figs. 22 and 23) it may be concluded that this rather crude, but reasonable, design method is quite satisfactory despite its simplicity.

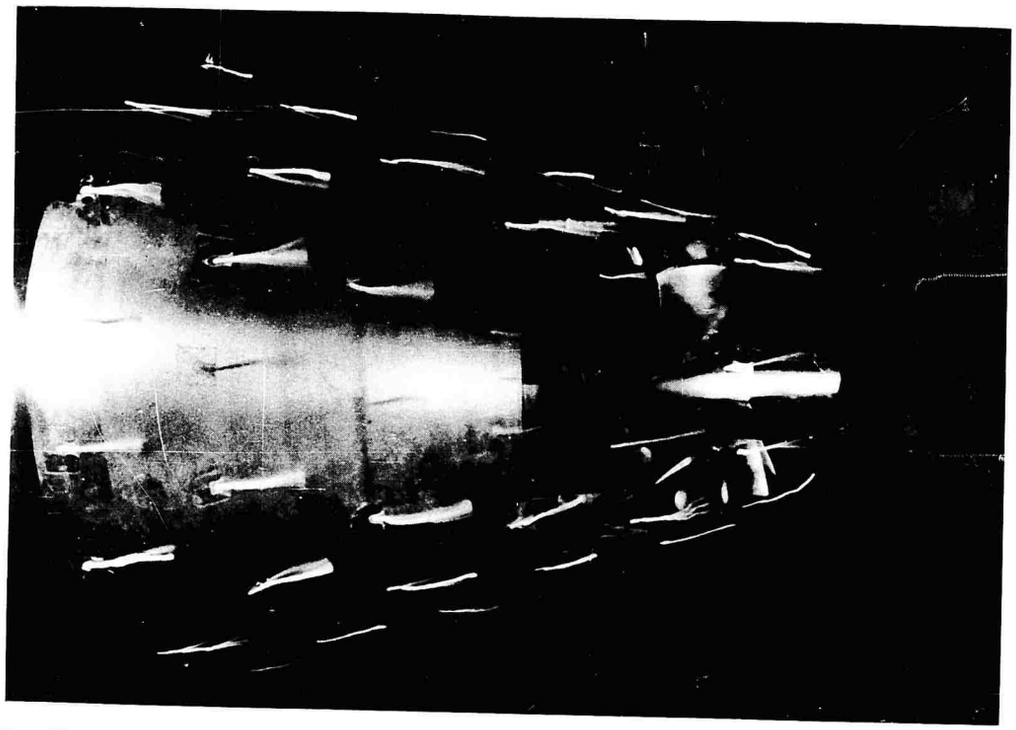

Fig. 22 - Flow Separation over Outer Surface of Pumpjet Shroud with No Rotation of the Rotor

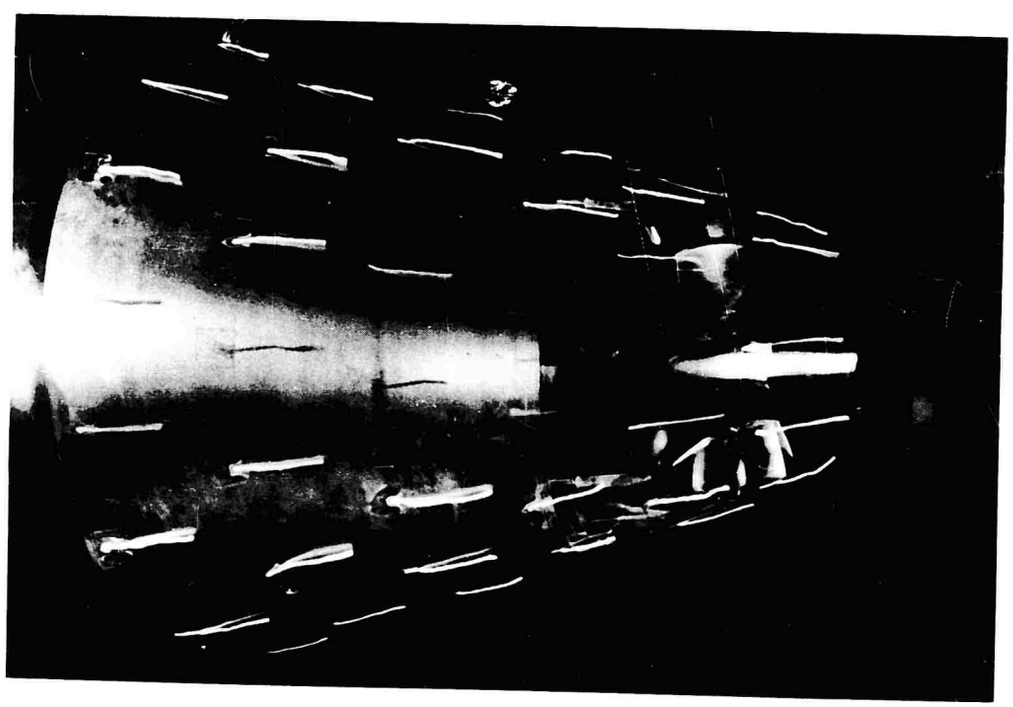

Fig. 23 - Flow over Outer Surface of Pumpjet Shroud with Rotor Operating

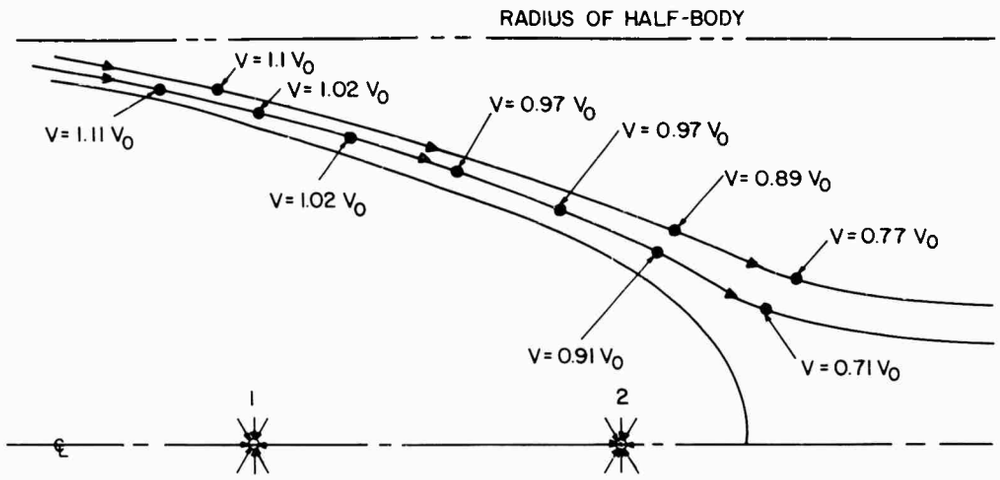

Fig. 24 - Streamline Pattern of Uniform Stream and Two Sinks

J. Internal Design of a High-Speed Pumpjet with Boundary-Layer Intake

INLET VELOCITY PROFILE

The pumpjet chosen to demonstrate this design method was originally designed for a torpedo-shaped test body 10 ft long and 21 in. in diameter. It was assumed that the intake of the pumpjet would be about 9 ft from the nose of the body, and the skin-friction drag coefficient up to this point was assumed to be 0.0045. Thus, the boundary-layer-momentum thickness (assuming a constant-diameter body) can be determined as follows:

$$\text{skin-friction drag} = 0.0045\,\rho\,\frac{V_0^2}{2}\,\pi\,d_0 L = \rho V_0^2 \theta \pi\, d_0, \tag{43}$$

where θ is the momentum thickness. Thus,

$$\theta = 0.0045\,\frac{L}{2} \tag{44}$$

Furthermore, it was assumed that the boundary-layer form factor was 1.35, which is representative of a turbulent boundary layer after having undergone a slight adverse pressure gradient. If a length L of 9 ft is used, the resulting over-all boundary-layer thickness is 2.235 in. For the particular example used here, the afterbody is already tapering at a point 9 ft from the nose; therefore, this thickness of 2.235 in. is somewhat fictitious. This boundary-layer thickness was then related to the diameter actually existing at 9 ft by a constant-area consideration.

This method of determining the boundary-layer thickness suffices for a first design when no experimental data exist on the body in question. If experimental data are available, both the boundary-layer thickness and velocity profile can, of course, be determined with greater precision by several methods.

The flow rate can now be determined by using the criterion of inducting 20 per cent of the boundary layer (incidentally, this 20 per cent figure also was determined by using a boundary-layer profile with a form factor of 1.35), thus yielding a pumpjet that is as small as is feasible without a serious loss in efficiency. The afterbody was designed (using the streamlines determined in the previous section) in a manner such that the static pressure at the shroud inlet was equal to the free-stream static pressure.

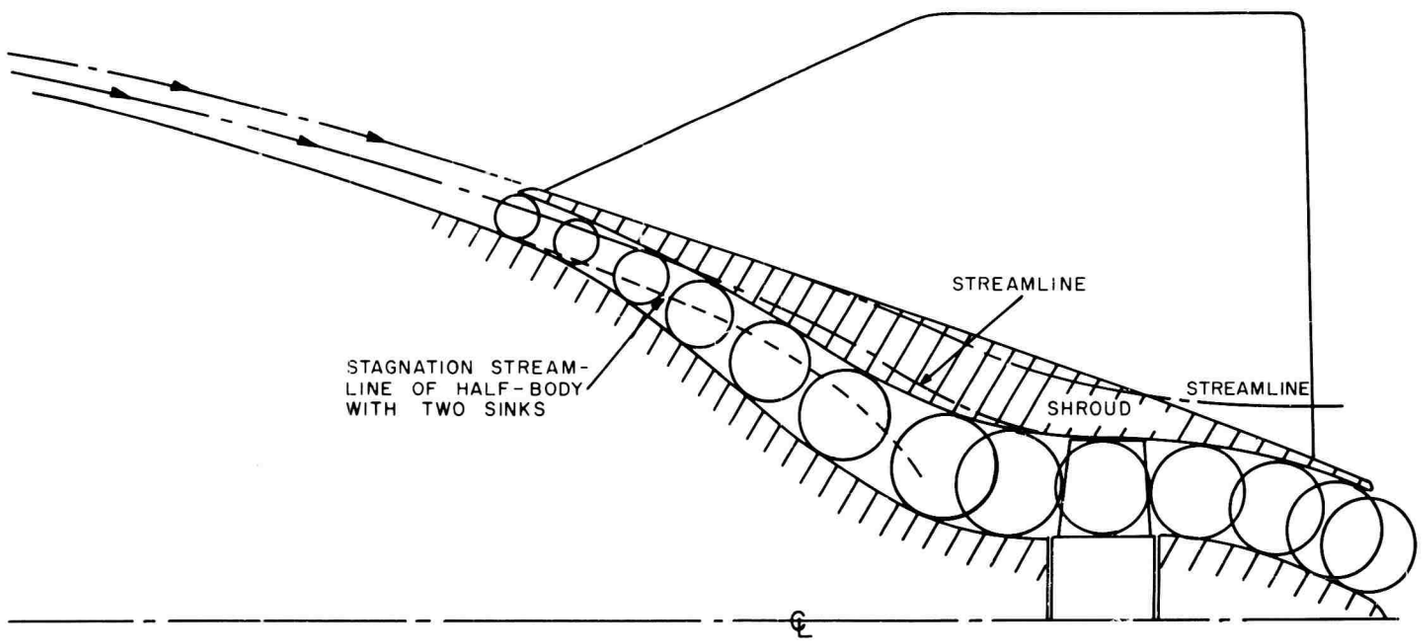

Fig. 25 - High-Speed-Pumpjet Shroud and Inlet Duct

VELOCITY PROFILES WITHIN THE SHROUD

Reference 3, which contains a design method for and a general description of boundary-layer intakes, states that some prediffusion ahead of the intake is both possible and desirable. This prediffusion tends to smooth out the rather abrupt pressure changes that seem to be unavoidable in intakes without prediffusion. Reference 3 indicates that about 15 per cent prediffusion leads to smooth pressure changes across the intake. Consequently, the inlet area was increased 15 per cent over that dictated by the 20 per cent criterion. In addition, the streamline for the outer contour of the shroud was chosen at a distance from the closed streamline dictated by this 15 per cent increase-in-area criterion. Reference 3 also indicates that boundary-layer intakes operate more efficiently if the initial diffusion is continued until velocities at the rotor inlet are lower than desired. The final stage of the inlet can then be similar to an accelerating nozzle, which is not only efficient but also tends to thin down the boundary layer on the inlet walls.

For this design, an inlet ram efficiency of 90 per cent was assumed; and reference 3 indicates that this is not unreasonable if the above points are considered.

The determination of the velocity profile at the inlet to the rotor completes the shroud design. Once the velocity profile at the inlet of the shroud is known, the profile at the rotor inlet can be determined in several ways. Perhaps the most direct is that given in reference 11. This method is based upon the fact that the vorticity remains constant along a streamline. It could be argued that the turbulent diffusion of vorticity could be significant in a long intake duct; however, the duct length in this design was assumed to be short compared to the length required for the development of a fully turbulent profile. This latter length should be a reasonable estimate for the distance required to significantly diffuse the vorticity.*

The profile determined as discussed above provides no information about the boundary-layer growth on the inside wall of the intake duct. It is possible for the boundary-layer growth to be sufficiently large to alter the predicted rotor inlet profiles. If the duct is designed such that there is an appreciable acceleration of the flow ahead of the rotor, this boundary-layer growth will be small and it can be accounted for by a slight enlargement of the duct. In the design described here, the flow was significantly accelerated; therefore, the area of the duct just ahead of the rotor was increased by 10 per cent over that used to determine the velocity profile. If it is suspected that there will be an appreciable boundary-layer growth, any of several methods of calculating turbulent boundary layers may be used. In particular, Schlichting's "Boundary Layer Theory" presents methods for calculating the turbulent boundary-layer growth on a body of revolution in an adverse pressure gradient.

ROTOR SIZE AND SPEED

In the previous discussion of the intake passage, the diameters of the rotor hub and the shroud were not determined. Obviously, these dimensions must be known before the passage can be designed. The selection of the rotor size and speed depends upon a number of factors. The relative importance of these factors depends upon the aims of the particular design; hence, no general statements can be made. The two factors that entered into the design in question were: a small, high-speed rotor; and acceptable cavitation performance.

The design can proceed in several ways. If a hub-to-tip diameter ratio is assumed for the rotor (0.5 was chosen for this design), then the rotor diameter determines the flow area through the rotor and, since the flow rate has already been determined, it also allows the axial velocity through the rotor to be calculated. Consequently, the pressure coefficient $2gH_R/U^2$ can be plotted as a function of $\overline{V_{m_2}}/U$ since

$$\frac{2gH_R}{U^2} = \frac{2gH_R}{\overline{V_{m_2}}^2} \frac{\overline{V_{m_2}}^2}{U^2}, \qquad 45$$

where $\overline{V_{m_2}}$ is the average meridional velocity at the rotor inlet.

*Tests with this pumpjet showed the total pressure distribution across the duct at the rotor inlet to be very nearly constant. Thus, it appears that there was a very appreciable turbulent diffusion.

If a single-stage propulsor is used, the pressure coefficient $2gH_R/U^2$ can go no higher than 0.40 or 0.45; otherwise, the blades will be loaded too heavily. In the case of a high-speed pumpjet, it is desirable that this coefficient be as low as possible because a low value implies a high rotational speed for a given head. By using Fig. 13, the cavitation number $2gH_{SV}/\overline{V_{m_2}}^2$ can be plotted vs $\overline{V_{m_2}}/U$ after the coefficient of minimum pressure on the blade is known. A reasonable assumption for the minimum pressure coefficient would be about 0.20 (0.23 was used in the present design). A better approximation of this value may be obtained after the blade pressure diagrams are determined and the process repeated. Note that the cavitation number decreases as $\overline{V_{m_2}}/U$ increases; i.e., a low pressure coefficient (high-speed rotor) and a low cavitation number (good cavitation performance) are opposite characteristics. After plotting both cavitation number and pressure coefficient vs $\overline{V_{m_2}}/U$, a compromise must be made between these two factors. For this particular design, $\overline{V_{m_2}}/U$ was chosen to be 0.32, which yielded a rather high pressure coefficient (0.43) and a rather high cavitation number (2.2).

If satisfactory values cannot be arrived at, another value for the rotor diameter can be selected and the pressure coefficient and cavitation number replotted. In this manner, the best possible compromise may be obtained. This completes the selection of the pumpjet parameters; only the design of the blade section remains. This step is carried out precisely as described in Section G.

K. Skewed Blading

THE EFFECT OF SKEWED BLADES

Perhaps the most radical innovation in the field of underwater propulsion since the introduction of pumpjets has been the use of skewed blades on propellers and on pumpjet rotors. The term "skew," as used here, describes the variation of a blade from a radial line when viewed in a direction along the axis of rotation of the propulsor. Also evident in some propulsor rotor blades is the existence of rake, which is defined as the variation of a blade in the fore-and-aft direction in the plane of the axis of rotation. Both of these properties are shown in Fig. 26.

In underwater propulsors such blades have been used in an attempt to reduce the unsteady forces generated by the propulsor and to improve its resistance to cavitation inception. The ability of a skewed blade to attain the former purpose is based upon the action of a blade when operating in a nonuniform through flow, such as that on a body of revolution just aft the fins or control surfaces. As the propulsor rotates, each blade moves through the viscous wakes produced by each control surface and reacts in much the same manner as an airplane wing reacts to a varying gust. The generation of unsteady forces resulting from such two-dimensional motion is known and has been treated analytically (12). Since the velocity deficiency caused by a control surface is usually distributed radially by virtue of the shape of the control surface, skew has been introduced to the propulsor blading to allow each blade to slice smoothly through the radial nonuniformity. This slicing action is in contrast to the action of an unskewed blade that suddenly encounters the control-surface wake along the entire length of the blade. The passage of a skewed blade through a control-surface wake is shown in Fig. 26.

The increased resistance to cavitation afforded by blade skew is analogous to the increase in critical Mach number associated with the swept-wing airplane. Because the leading edge of the wing is at an angle to the air flow, components of velocity exist that are parallel to and normal to the leading edge. In a swept wing, the sections can be thought of as "seeing" only the velocity normal to the leading edge. Then, two-dimensional blade-section design data can be used. Thus, the swept wing (compared with an unswept wing) reduces the blade loading by a factor equal to the cosine squared of the swept angle (see Fig. 27). As a result of this reduction in loading, there will also be a reduction in velocity over the section and, therefore, a lower critical Mach number. The analogy between critical Mach number and cavitation resistance indicates, therefore, an increased resistance to cavitation as the result of introducing skew to rotating blades.

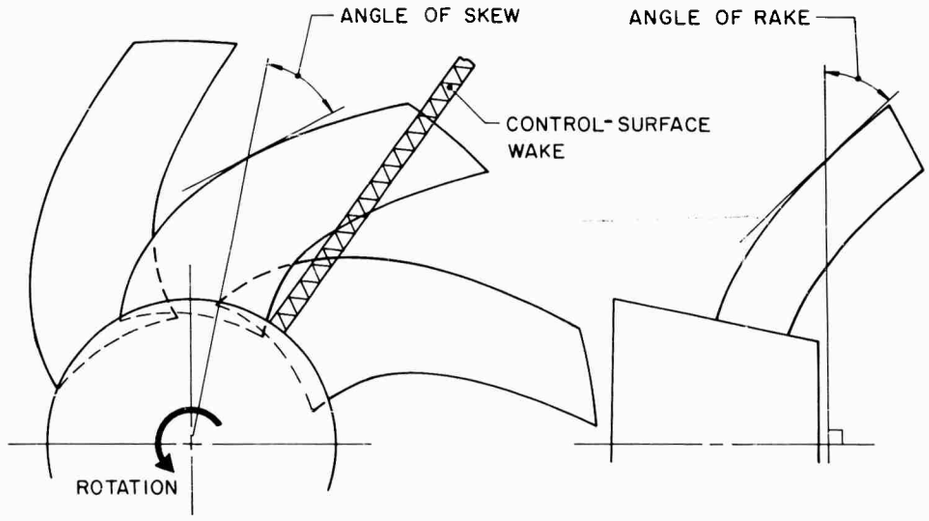

Fig. 26 - Rotor Blades that Are both Raked and Skewed

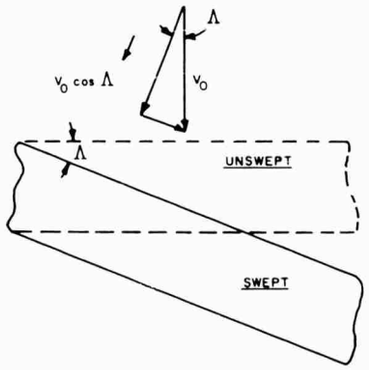

Fig. 27 - Two-Dimensional Effect of Skew

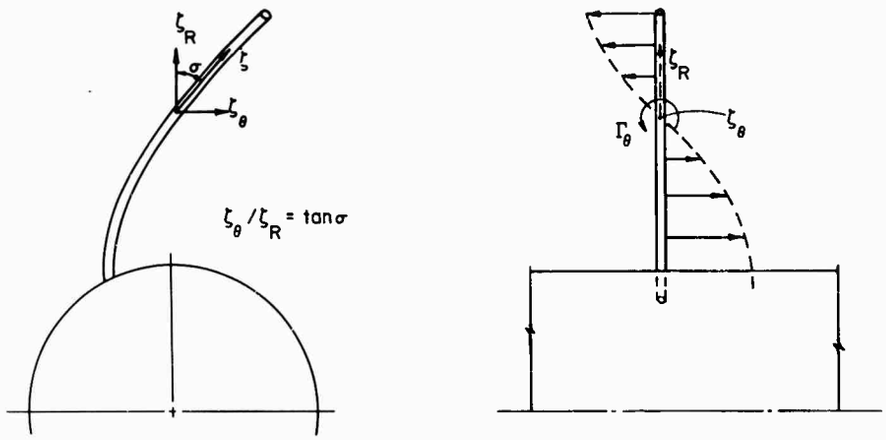

Fig. 28 - Skewed Bound Vortex Line and Its Effect on Meridional Flow

SKEW EFFECT AND VELOCITY PROFILES

Because it is highly advantageous to consider the flow through a rotating propulsor blade along an axisymmetric flow surface or along approximate flow surfaces (as discussed above), the application of two-dimensional cascade data for the design of a skewed-blade propulsor is not possible without certain corrections. These corrections, which are required as a consequence of the spanwise flow introduced by the presence of skew, are presented in detail in reference 13; therefore, they will not be repeated in this report. Reference 13 also includes a discussion of the effect at the ends of a skewed blade caused by the presence of the shroud and the hub. This effect will be discussed later in this report.

The design of skewed blades as presented in reference 13 assumes that the flow field entering and leaving such a blade is known. The flow through a skewed blade is much different from that for an unskewed blade, as can be seen from Fig. 28. In this figure, the action of the skewed blade is replaced by a bound vortex line having a total vorticity of ζ. The total vorticity will have both a radial component ζ_R and a circumferentially directed component ζ_θ. If the blade also has rake, an axial component will also exist. It is assumed, for the present, that the blade has no rake and, therefore, no axial component. The effect of the radially directed vorticity is, by itself, the same as that which exists in an unskewed blade. The circumferential component thereby represents the effect of skew on the flow field through the propulsor.

If an axisymmetric flow field or an infinite number of blades is assumed, the circumferential vorticity will appear as a continuous radial distribution of ring vortices concentric about the axis of rotation. The circulation of each ring vortex is related to ζ_θ by the definition of vorticity, i.e., circulation per unit area - which is, in turn, related to ζ_R by the skew angle σ. Therefore, if the value of ζ_R required to produce the necessary turning or rotor thrust is known, the distribution of ring vortex circulation, γ_θ, is known.

To illustrate the action of these vortices, consider the radial distribution replaced by a single ring vortex of strength

$$\Gamma_\theta = \int_{R_{HUB}}^{R_{TIP}} \gamma_\theta \, dR \qquad 46$$

The effect of such a vortex on the meridional flow in the plane of the leading or trailing edge of the blade (the vortex is positioned at the midchord of the blade) is shown in Fig. 28b. It is seen to be an effect of increasing the through-flow velocity near the hub of the rotor and decreasing it near the blade tip.

With the introduction of a shroud to the skew-bladed rotor, the condition of zero velocity normal to the shroud must be satisfied. A similar condition must be maintained at the hub surface. If both the shroud and the hub surface are approximated by cylindrical surfaces (concentric cylinders about the axis of rotation) then, by unwrapping the flow surface and considering it as a plane rather than axisymmetric flow, these boundary conditions can be satisfied. The effect of ζ_θ on the meridional velocity becomes the solution for an infinite row of two-dimensional vortices with the shroud and the hub surface represented by the straight dividing streamlines between adjacent vortices. A more accurate approximation of the effect of ζ_θ then follows by replacing the single vortex of strength Γ by a continuous but still two-dimensional distribution of vortices of strength γ_θ between the hub and shroud.

The use of a distribution of two-dimensional vortices in place of a distribution of axisymmetric ring vortices is an expediency necessitated by the lack of a straightforward solution for the proper dividing streamlines. It is of interest to note, however, that the use of a finite number of ring vortices - together with a distribution of sources or sinks on the axis of rotation - has been employed successfully for the design of a skew-bladed propeller. Future work should include an attempt to obtain a more realistic representation of this effect in pumpjets.

After obtaining the velocity distribution representing the effect of skew (see Fig. 28b), the distribution must be corrected to assure that the condition of continuity is satisfied. This correction requires the nodal point of the velocity distribution, or the point where the velocity changes direction, to be shifted either inboard or outboard in a manner such that the portion of axial velocity induced aft represents the same mass flow as that induced forward. The resulting velocity distribution is then added to that associated with ζ_R, and the blade design can proceed since the entire velocity field is known.

TIP EFFECTS

The introduction of skew to the rotor of a pumpjet has resulted in an interaction problem not previously significant in pumpjets: the interaction of the rotor tip and the boundary layer on the inside of the shroud. By virtue of the induced velocity representing the effect of skew, a retardation of the boundary layer occurs on the inside of the shroud. Such a retardation subjects the tip of the rotor blades to a high local angle of attack resulting in a high loading at the leading edge of the section. As a result, the leading edge will exhibit very localized cavitation.

There appear to be several approaches to control this high loading and the resulting cavitation. One method is to control the amount of retardation by limiting the velocity induced by the introduction of skew. This procedure results in an upper limit on the value of the skew angle σ It appears, on the basis of experimental observations, that if the forward axial velocity induced by ζ_θ is maintained - so as not to exceed 20 per cent of the total axial velocity without skew - then an excessive amount of retardation will not occur. Previous mention has been made of the material presented in reference 13 concerning the blade and the effects of enclosing a skewed blade in a shroud or casing. This effect is included by representing the action of the blade by a vortex system with an image vortex system to represent the effects of the wall. With such a vortex representation, the additional induced velocities resulting from the presence of the wall can be determined and included with the previously determined velocity field.

The representation of the blades and shroud in reference 13 assumes a two-dimensional flow. The existence of a curved rather than a plane wall in a pumpjet, therefore, makes this approach a first approximation. The results of this study do show, however, the need for introducing additional camber to the tip section of the blade, which is in agreement with experimental observations that indicate a high localized loading at the blade leading edge.

L. Experimental Results

The previously discussed design principles and procedures have been employed at the Ordnance Research Laboratory for the design of pumpjets to be used for the propulsion of completely sub-

merged, axisymmetric bodies. Applications of low-speed pumpjets have been made for both torpedoes and submarines, and high-speed pumpjets have been applied to torpedoes.

A LOW-SPEED PUMPJET OPERATING ON THE AFTER END OF A BODY OF REVOLUTION

The experimental results obtained with a low-speed pumpjet are typified by those for an 8-in.-diameter torpedo model. The general arrangement of this pumpjet is as shown in Fig. 14. The results of water-tunnel tests conducted on this propulsor are shown in Figs. 29 and 30. The design advance ratio for this propulsor was 1.725 as compared to the operating advance ratio of 2.025. The operating advance ratio is defined as the advance ratio at which the net thrust is zero. This discrepancy between the design and operating advance ratios is due primarily to two reasons:

1. The original drag coefficient was overestimated. (This propulsor was designed before accurate wake data could be obtained from the model.) This experience emphasizes the need for accurate wake data, but the lack of such data does not present a basic problem.

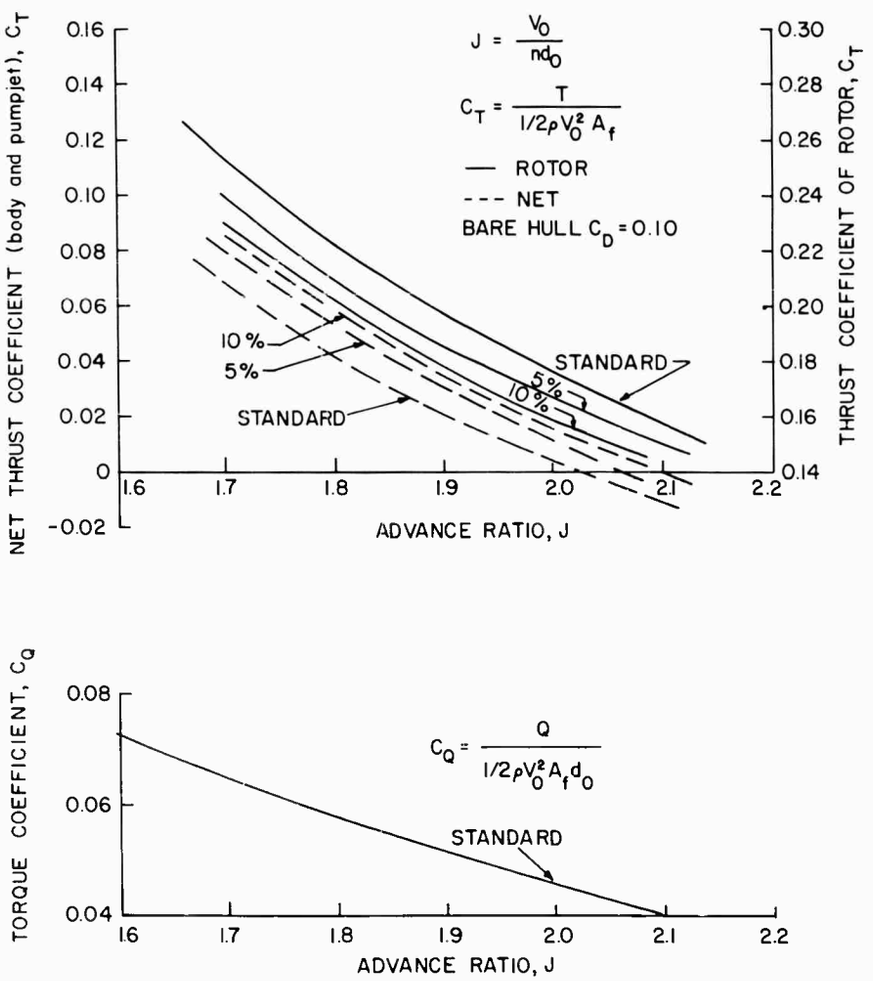

Fig. 29 - Thrust and Torque Coefficients as a Function of Advance Ratio

2. No adequate method of determining the alteration of the drag resulting from the presence of the pumpjet is available. It is felt that the analytic determination of this effect is, as yet, the most important problem remaining in pumpjet design.

Figure 29 demonstrates the advantage of model tests. The curves designated "5 per cent" and "10 per cent" represent an increase in shroud exit area by the amount indicated in contrast to the as-designed exit-area curve designated "standard." The variation in net thrust as the result of these increases in exit area demonstrates how the performance of a pumpjet can be altered by such minor modifications.

The overestimation of the design thrust can be termed an advantage with respect to the cavitation performance of the propulsor. The observed critical cavitation indexes of the unit as a function of advance ratio are shown in Fig. 30. The curves marked "unmodified" represent the cavitation performance of the pumpjet as observed with the blading in its original or as-designed form. Observations with the blades in this form indicated premature suction-surface cavitation on their leading edges. A modification to the blades, based on the acutal wake data, consisted of an increase in the slope of the mean camber line by approximately 5 deg in the vicinity of the leading edge. The resulting cavitation data are indicated "modified." This improvement, together with the increase of the self-propulsion advance ratio to 2.025, resulted in a cavitation performance that exceeds the predicted critical index of approximately 0.7.

A HIGH-SPEED PUMPJET OPERATING ON THE AFTER END OF A BODY OF REVOLUTION

Considerable experimental data have been obtained on the high-speed pumpjet described in Sections I and J. These data are presented in detail in reference 14. Figure 31 shows a plot of

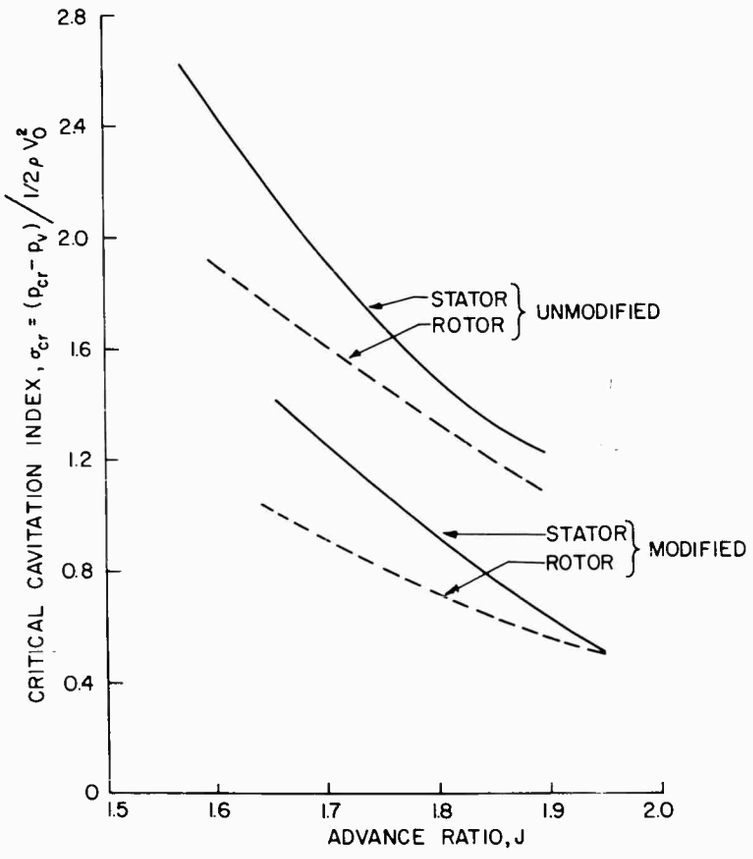

Fig. 30 - Cavitation Performance of a Pumpjet

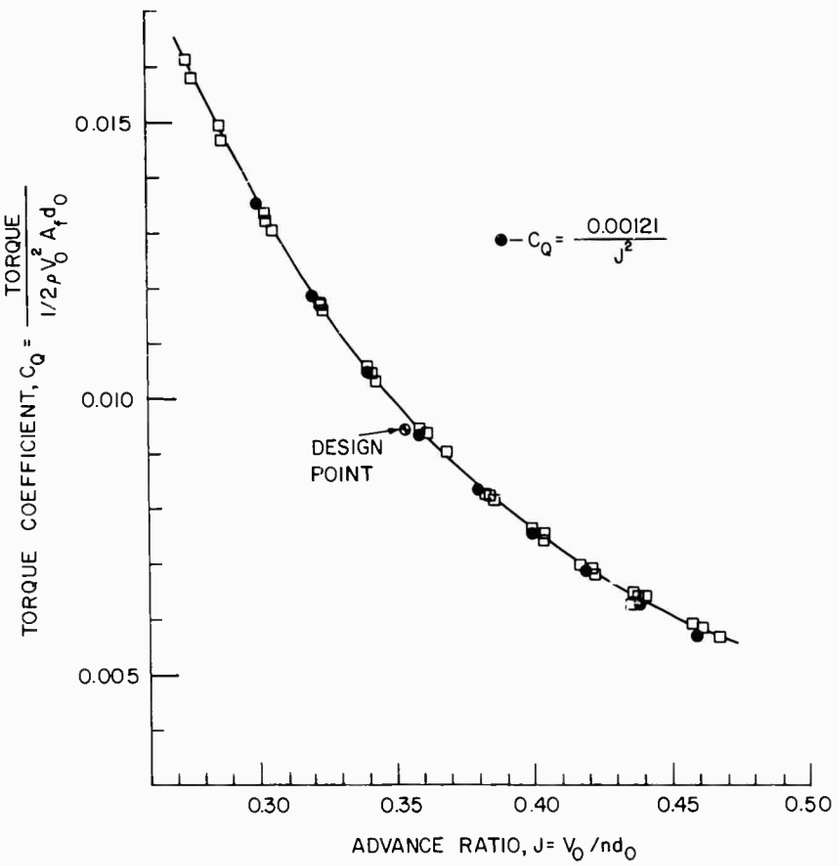

Fig. 31 - Torque Coefficient as a Function of Advance Ratio for the High-Speed Pumpjet

torque coefficient vs advance ratio with the design point indicated. The fact that the design point lies very close to the actual operating curve indicates the adequacy of the design method described in this report. The operating advance ratio (not shown) was approximately 7 per cent higher than the design advance ratio (indicating an overdesign), thus demonstrating a basic inadequacy in estimating the drag.

The velocity profile measured at the rotor inlet of the propulsor is shown in Fig. 32. The rapid velocity decrease near the hub and near the shroud represents the boundary-layer growth on the hub and shroud surfaces. The thickness of the shroud boundary layer results in excessive angles of attack near the tip of the blade and is manifested by poor cavitation performance at the blade tip. The velocity profiles designated "design" were determined assuming that the energy distribution across the flow was the same at the rotor inlet as it was at the shroud inlet. The velocity profile designated "uniform energy distribution" was determined assuming that the nonuniform energy distribution at the shroud inlet was completely "smeared out" before the flow reached the rotor inlet. The curve for uniform energy distribution is obviously more accurate than the design curve.

The cavitation performance of this pumpjet is shown in Fig. 33. The blade-surface cavitation near the midspan of the blades is about as predicted in the design analysis; however, the important point is that the most critical regions (with respect to cavitation performance) are: (a) the leading-edge suction surface at the tip of the blade (this is a result of the shroud boundary layer discussed above), and (b) the leadage vortex caused by the leakage flow across the blade tip. Both phenomena

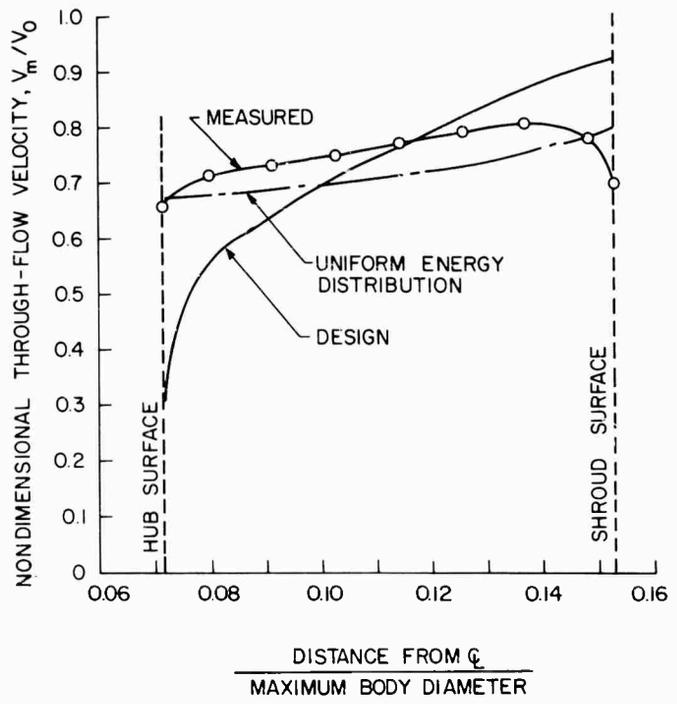

Fig. 32 - Velocity Profile at Rotor Inlet of the High-Speed Pumpjet Operating at Design Conditions

are caused by the interaction between the rotor and the shroud and, hence, are inherent to pumpjets. It is the authors' opinion that this interaction represents a major unsolved problem in pumpjets.

M. Conclusions and Recommendations

At the Ordnance Research Laboratory, the hydrodynamic design of pumpjets for the propulsion of underwater vehicles is aimed primarily toward the attainment of a high resistance to cavitation in the propulsor, and such performance has been demonstrated. Three factors have been responsible for the success of this program.

1. The NACA cascade data, in their original form, are not satisfactory for the design of a pumpjet with high cavitation resistance. By a judicious generalization of these data, blade-section profiles were obtained that are more uniformly loaded along their chord than the NACA profiles.

2. High-solidity blading was used to increase the number of blades and to reduce the loading on each blade. This improvement is achieved at the sacrifice of efficiency because of the added skin-friction drag, but this efficiency loss must be accepted to obtain high cavitation resistance.

3. The velocity profiles at the inlet and exit of the rotor and stator blades were carefully determined.

The authors believe that the hydrodynamic design of pumpjets includes problems that are not completely solved. The major problems are listed below.

1. Means must be found to predict the effect of the shroud on the net force produced by the propulsor and on the flow through the propulsor. Such work should supplement the work of reference 7 and may include the work of reference 5.

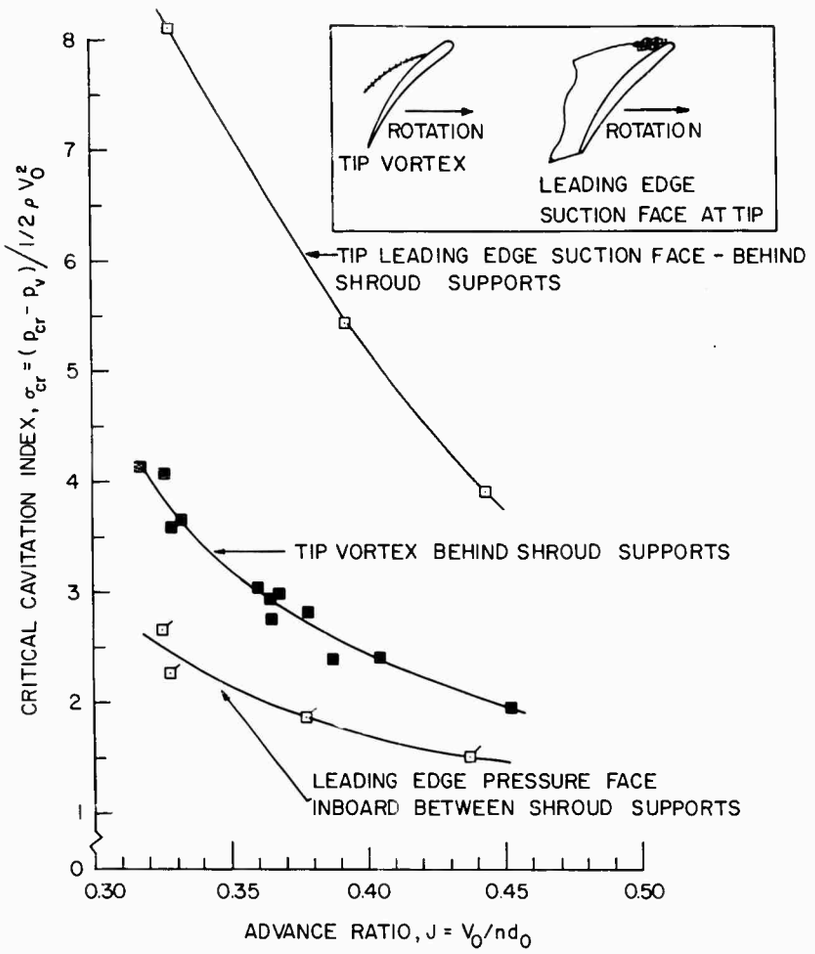

Fig. 33 - Cavitation Performance of the High-Speed Pumpjet

2. Detailed experimental and analytical investigations of the flow near the tips of the rotor blade are required to determine the effect of the presence of shroud and the clearance between the shroud and blade ends.

3. Unsteady flow and unsteady forces are problems that are common in the design of both pumpjets and propellers.

References

(1) George F. Wislicenus, Principles and Applications of Bypass Turbojet Engines, SAE Transactions, Vol. 64, 1956, p. 486.

(2) George F. Wislicenus and L. H. Smith, Hydraulic Jet Propulsion and Incipient Cavitation, Johns Hopkins University, Institute for Cooperative Research, Report I-6, Part A, March 21, 1952.

(3) S. J. Eskinazi, C. D. Flagle, R. Ruetenik, and J. R. Weske, A Problem in Retardation of a Turbulent Boundary Layer, Johns Hopkins University, Institute for Cooperative Research, Report I-6, Part B, March 21, 1952.

(4) Members of Compressor and Turbine Research Division of Lewis Flight Propulsion Laboratory, NACA, Aerodynamic Design of Axial-Flow Compressors, Lewis Flight Propulsion Laboratory Reports NACA RM E56BO3, NACA RM E56BO3a, and NACA RM E56BO3b, August 1, 1956.

(5) H. E. Dickman (Translation by Finkelstein, Meyerhoff, and Facharkiw), Fundamentals of Annular Airfoil Theory (Nozzles in a Free Stream), PIBAL Report No. 353, August 1956.

(6) D. Kuchemann and J. Weber, Aerodynamics of Propulsion, McGraw-Hill Book Company, New York, 1953.

(7) B. W. McCormick and J. J. Eisenhuth, The Design and Performance of Propellers and Pumpjets for Underwater Propulsion, Journal of the American Institute of Aeronautics and Astronautics, Vol. 1, No. 10, October 1963, pp. 2348-2354.

(8) E. A. Eichelbrenner at al., Theoretical Investigation and Control by Measuring Tests on the Behavior of a Three-Dimensional Turbulent Boundary Layer on an Annular Wing at Various Incidences, Prepared for ONR by Bureau Technique Zborowski, France, December 1961.

(9) George F. Wislicenus, Hydrodynamics and Propulsion of Submerged Bodies, Journal of the American Rocket Society, Vol. 30, No. 12, December 1960, pp. 1140-1148.

(10) George F. Wislicenus, Fluid Mechanics of Turbomachinery, McGraw-Hill Book Company, 1947. Revised edition to be published by Dover Publications, Inc., New York.

(11) L. H. Smith, S. C. Traugott, and G. F. Wislicenus, A Practical Solution of a Three-Dimensional Flow Problem of Axial-Flow Turbomachinery, Transactions of the American Society of Mechanical Engineers, Vol. 75, No. 5, July 1953.

(12) W. R. Sears, Some Aspects of Non-Stationary Airfoil Theory and Its Practical Application, Journal of Aeronautical Sciences, Vol. 8, No. 3, September 1941.

(13) L. H. Smith and H. Yeh, Sweep and Dihedral Effects in Axial-Flow Turbomachinery, American Society of Mechanical Engineers Paper No. 62-WA-102, 1962.

(14) W. S. Gearhart and R. E. Henderson, Results of Experimental Investigations with a High Speed, Boundary Layer Intake Pumpjet, Ordnance Research Laboratory Technical Memorandum TM 506.3810-02, January 31, 1964.

APPENDIX

Blade-Layout Diagrams

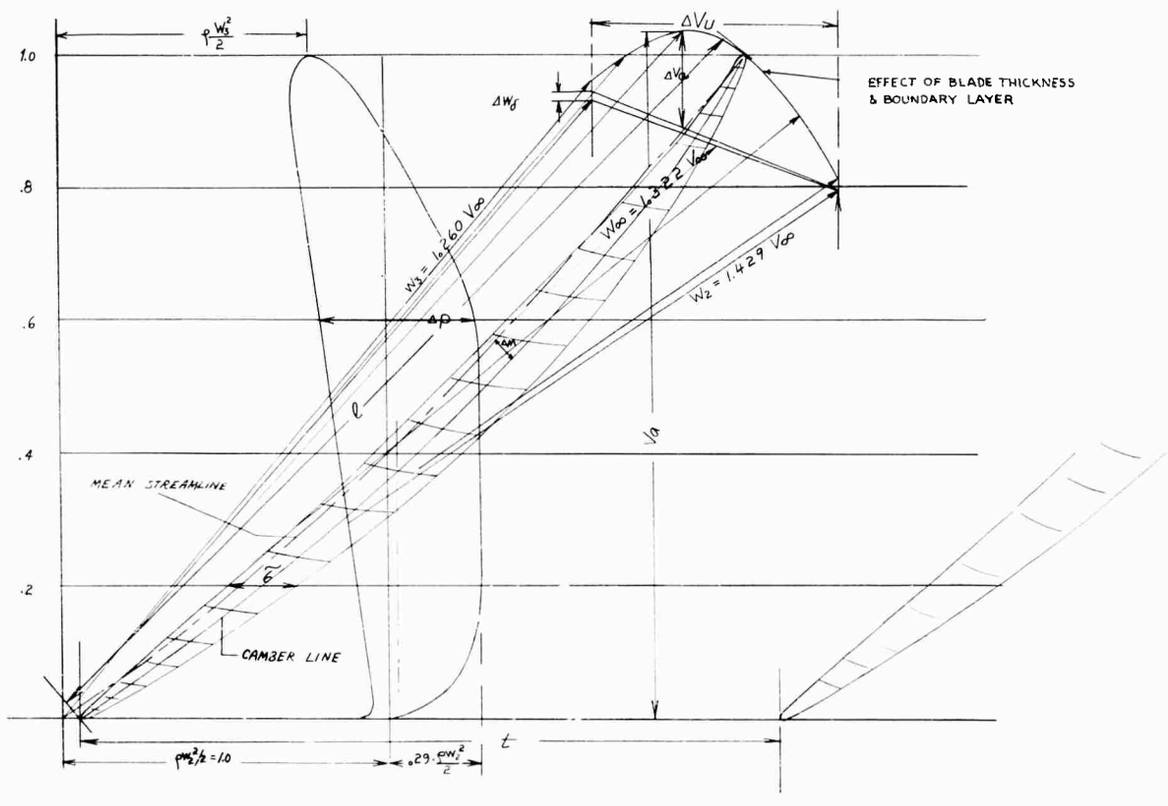

A - Typical Section of a Blade with a High Advance Ratio

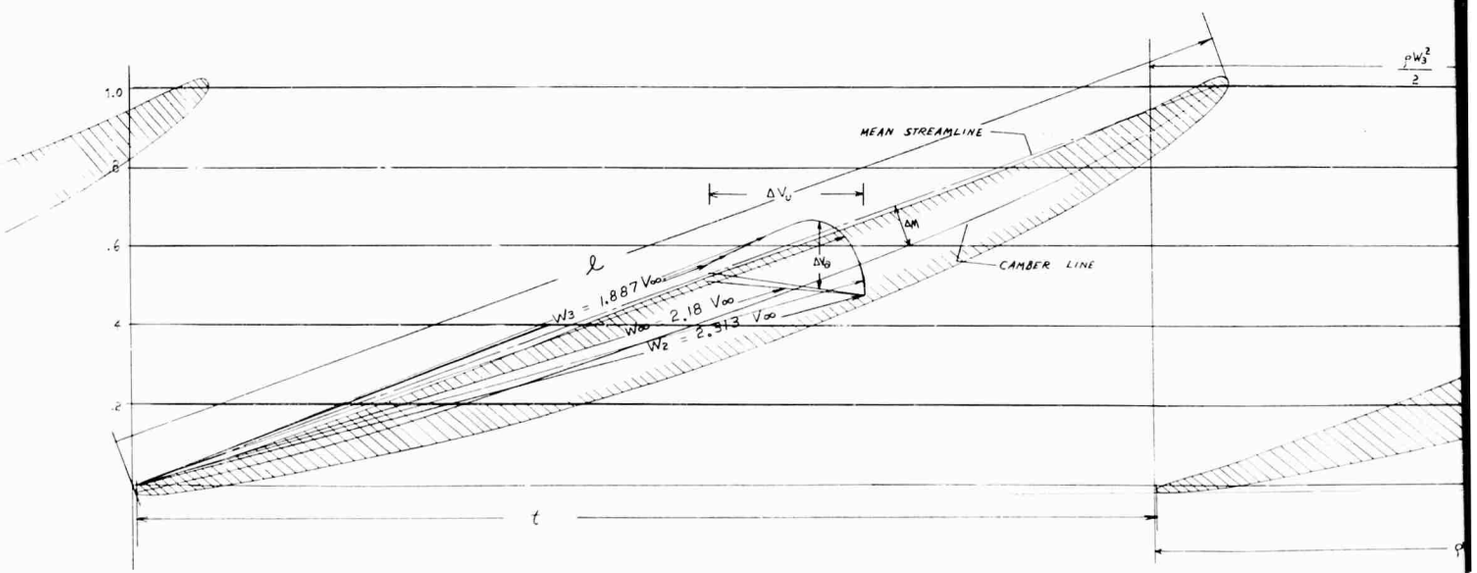

B - Tip Section of a Blade with a Low Advance Ratio

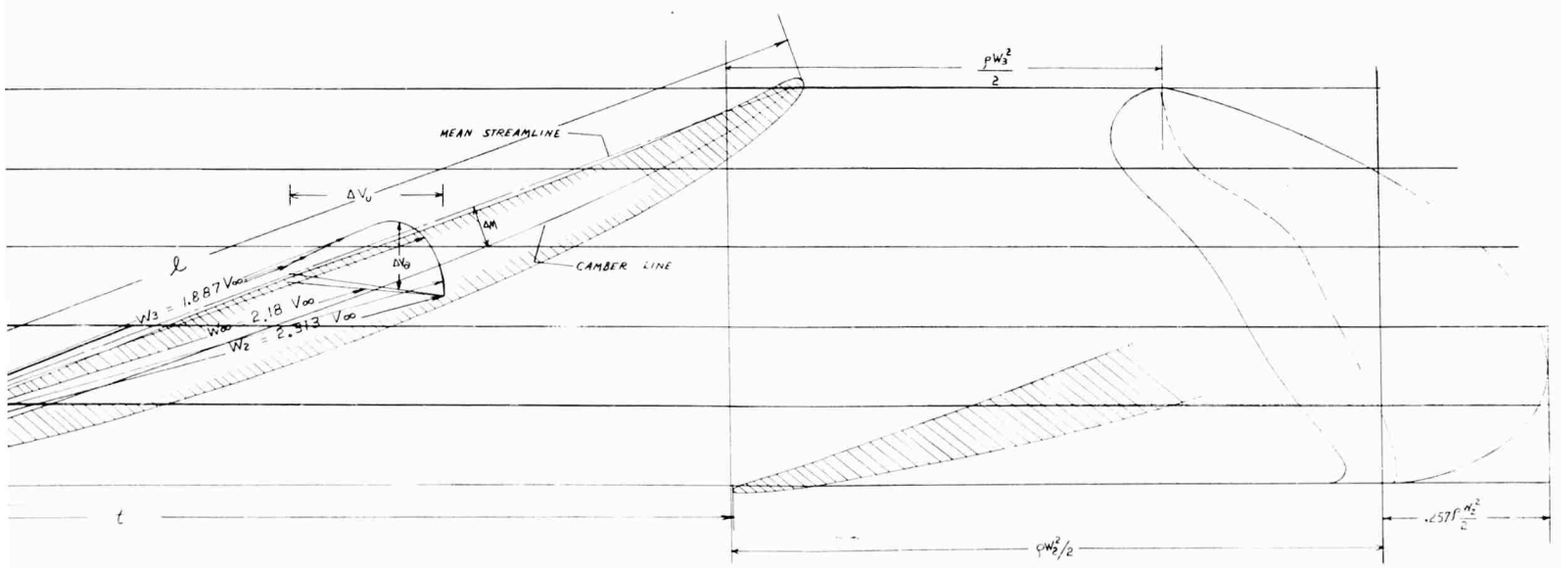

B - Tip Section of a Blade with a Low Advance Ratio

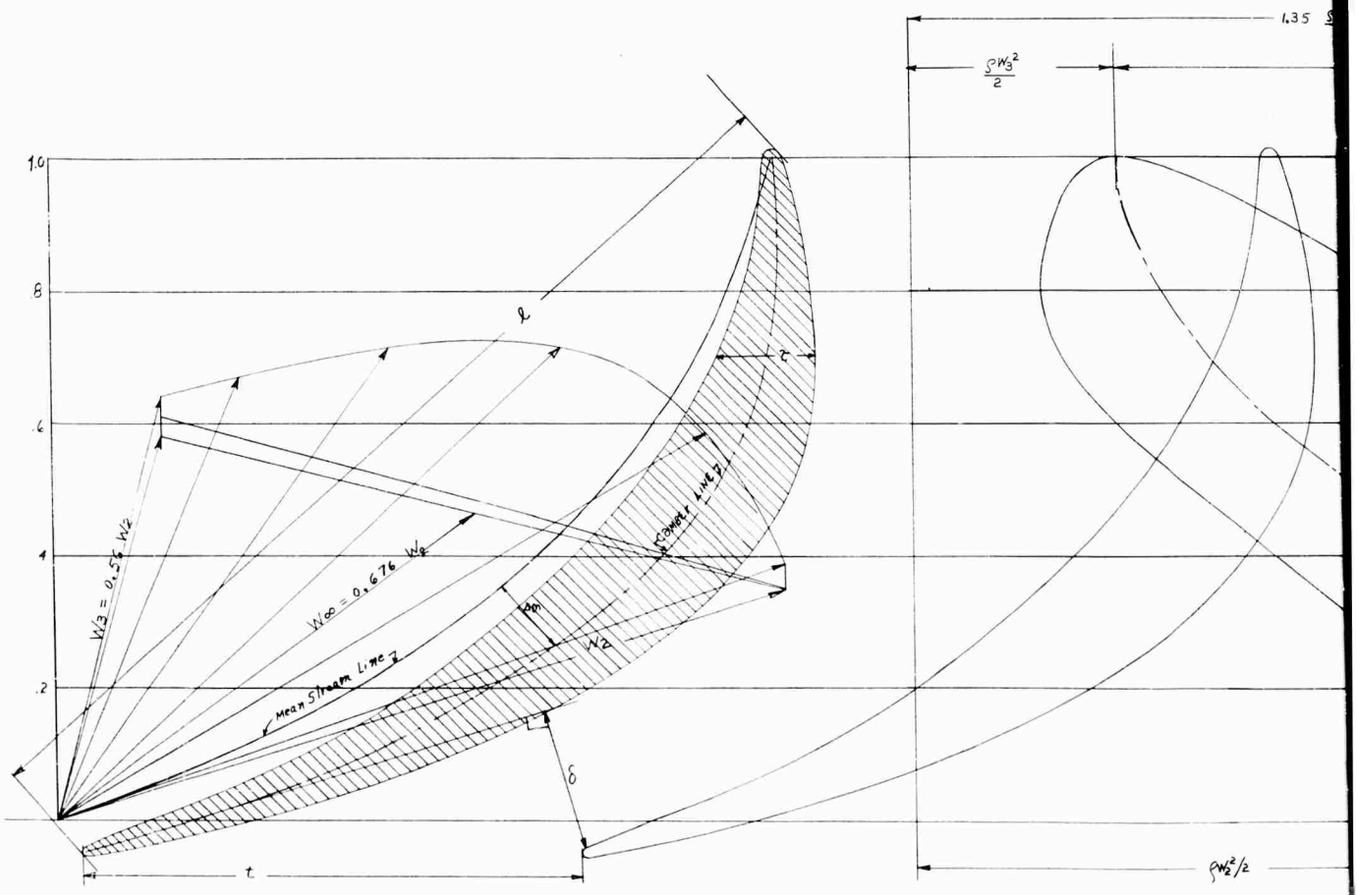

C - Root Section of a Blade with a Low Advance Ratio

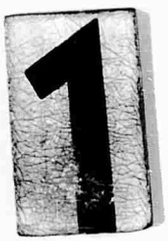

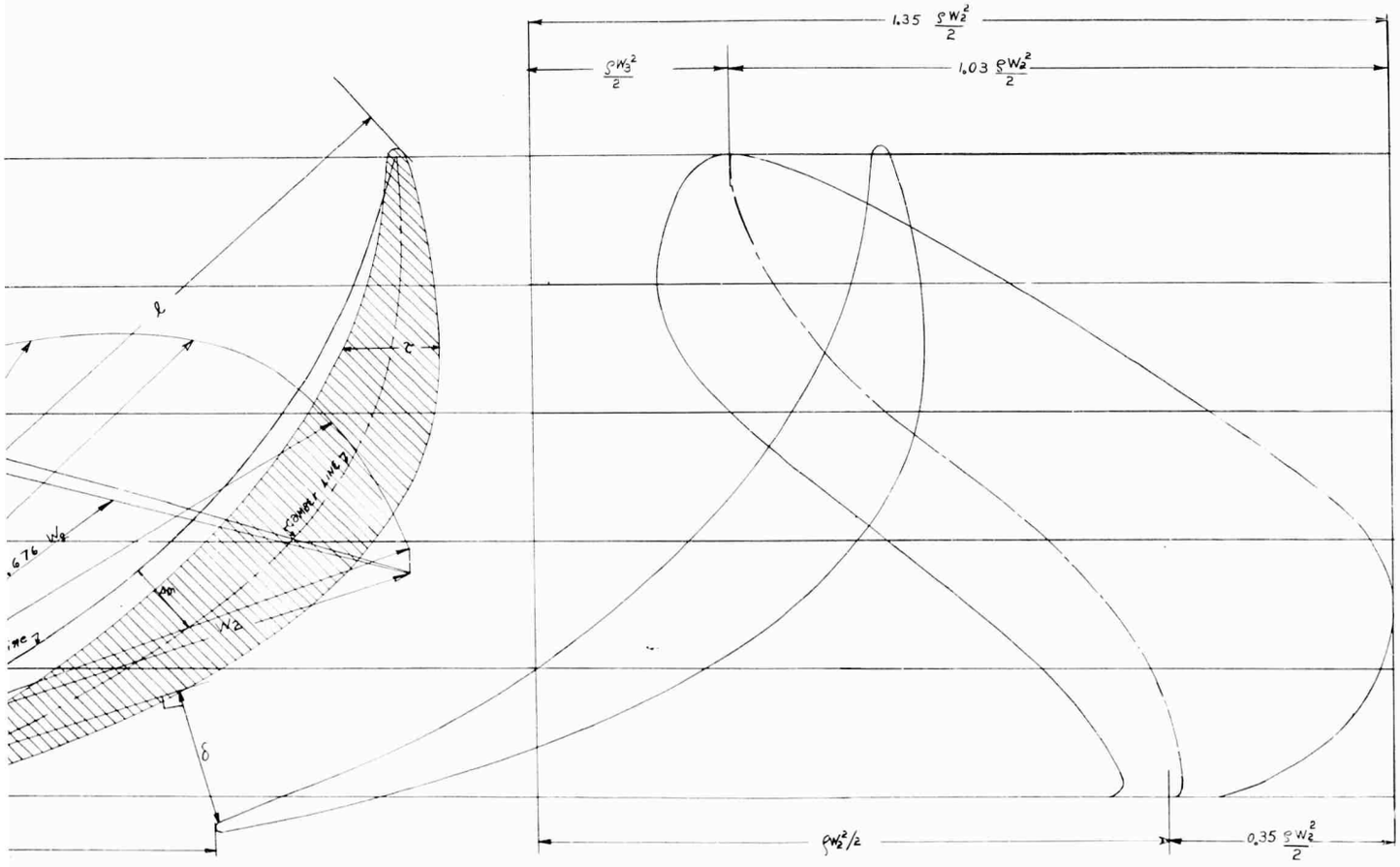

C - Root Section of a Blade with a Low Advance Ratio

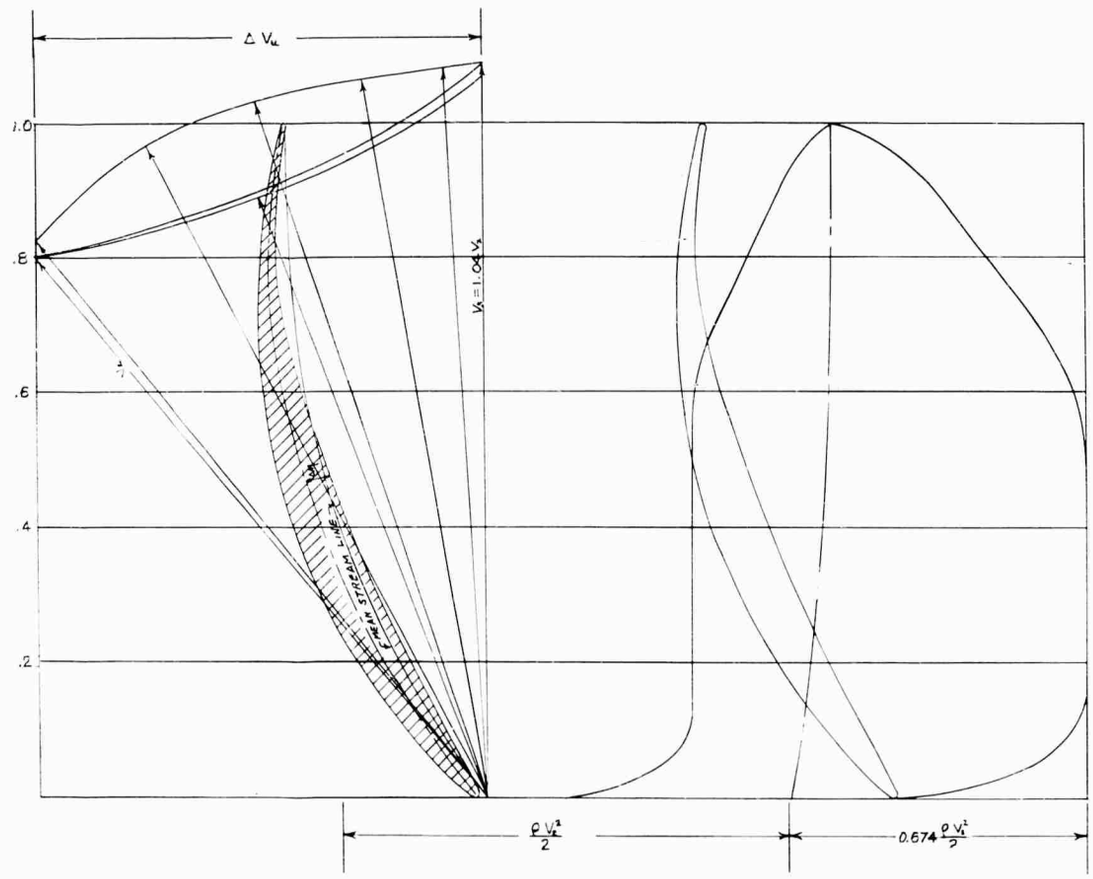

D - Typical Diffuser-Blade Section

This card is UNCLASSIFIED

Ordnance Research Laboratory Report No. NOw 63-0209-c-7
The Pennsylvania State University, University Park, Pa.

A METHOD FOR THE DESIGN OF PUMPJETS

This report is UNCLASSIFIED

R. E. Henderson, J. F. McMahon, and G. F. Wislicenus

May 15, 1964; 45 pp. & figs.

The pumpjet - a hydrodynamic propulsor - is similar to a conventional propeller rotating within a duct or shroud. The shroud permits the flow velocity through the rotor to be controlled more or less independently of the velocity of the vehicle. For certain applications, the pumpjet can be designed to have better cavitation characteristics than an open propeller; alternatively, the pumpjet can be made smaller than the conventional propeller to reduce the weight of the propelling machinery.

The pumpjet may be designed on the basis of knowledge and experience gained from axial-flow compressors and pumps. The meridional flow within the shroud is assumed to be axially symmetrical. The flow through the vane system is considered, with certain restrictions, to be cy-

(over)

This card is UNCLASSIFIED

Ordnance Research Laboratory Report No. NOw 63-0209-c-7
The Pennsylvania State University, University Park, Pa.

A METHOD FOR THE DESIGN OF PUMPJETS

This report is UNCLASSIFIED

R. E. Henderson, J. F. McMahon, and G. F. Wislicenus

May 15, 1964; 45 pp. & figs.

The pumpjet - a hydrodynamic propulsor - is similar to a conventional propeller rotating within a duct or shroud. The shroud permits the flow velocity through the rotor to be controlled more or less independently of the velocity of the vehicle. For certain applications, the pumpjet can be designed to have better cavitation characteristics than an open propeller; alternatively, the pumpjet can be made smaller than the conventional propeller to reduce the weight of the propelling machinery.

The pumpjet may be designed on the basis of knowledge and experience gained from axial-flow compressors and pumps. The meridional flow within the shroud is assumed to be axially symmetrical. The flow through the vane system is considered, with certain restrictions, to be cy-

(over)

This card is UNCLASSIFIED

Ordnance Research Laboratory Report No. NOw 63-0209-c-7
The Pennsylvania State University, University Park, Pa.

A METHOD FOR THE DESIGN OF PUMPJETS

This report is UNCLASSIFIED

R. E. Henderson, J. F. McMahon, and G. F. Wislicenus

May 15, 1964; 45 pp. & figs.

The pumpjet - a hydrodynamic propulsor - is similar to a conventional propeller rotating within a duct or shroud. The shroud permits the flow velocity through the rotor to be controlled more or less independently of the velocity of the vehicle. For certain applications, the pumpjet can be designed to have better cavitation characteristics than an open propeller; alternatively, the pumpjet can be made smaller than the conventional propeller to reduce the weight of the propelling machinery.

The pumpjet may be designed on the basis of knowledge and experience gained from axial-flow compressors and pumps. The meridional flow within the shroud is assumed to be axially symmetrical. The flow through the vane system is considered, with certain restrictions, to be cy-

(over)

This card is UNCLASSIFIED

Ordnance Research Laboratory Report No. NOw 63-0209-c-7
The Pennsylvania State University, University Park, Pa.

A METHOD FOR THE DESIGN OF PUMPJETS

This report is UNCLASSIFIED

R. E. Henderson, J. F. McMahon, and G. F. Wislicenus

May 15, 1964; 45 pp. & figs.

The pumpjet - a hydrodynamic propulsor - is similar to a conventional propeller rotating within a duct or shroud. The shroud permits the flow velocity through the rotor to be controlled more or less independently of the velocity of the vehicle. For certain applications, the pumpjet can be designed to have better cavitation characteristics than an open propeller; alternatively, the pumpjet can be made smaller than the conventional propeller to reduce the weight of the propelling machinery.

The pumpjet may be designed on the basis of knowledge and experience gained from axial-flow compressors and pumps. The meridional flow within the shroud is assumed to be axially symmetrical. The flow through the vane system is considered, with certain restrictions, to be cy-

(over)

lindrical. Although axial-compressor data can be used for the blade design, blade profiles suitable for compressors are not suitable for hydrodynamic propulsors because of the stringent requirements regarding cavitation. A quasi one-dimensional method of blade design is described that uses compressor data but still meets the cavitation requirements.

Problems of shroud design, skewed vanes, unsteady force action, and boundary-layer intake are discussed; and problems that remain unsolved are also pointed out.

lindrical. Although axial-compressor data can be used for the blade design, blade profiles suitable for compressors are not suitable for hydrodynamic propulsors because of the stringent requirements regarding cavitation. A quasi one-dimensional method of blade design is described that uses compressor data but still meets the cavitation requirements.

Problems of shroud design, skewed vanes, unsteady force action, and boundary-layer intake are discussed; and problems that remain unsolved are also pointed out.

lindrical. Although axial-compressor data can be used for the blade design, blade profiles suitable for compressors are not suitable for hydrodynamic propulsors because of the stringent requirements regarding cavitation. A quasi one-dimensional method of blade design is described that uses compressor data but still meets the cavitation requirements.

Problems of shroud design, skewed vanes, unsteady force action, and boundary-layer intake are discussed; and problems that remain unsolved are also pointed out.

lindrical. Although axial-compressor data can be used for the blade design, blade profiles suitable for compressors are not suitable for hydrodynamic propulsors because of the stringent requirements regarding cavitation. A quasi one-dimensional method of blade design is described that uses compressor data but still meets the cavitation requirements.

Problems of shroud design, skewed vanes, unsteady force action, and boundary-layer intake are discussed; and problems that remain unsolved are also pointed out.